UNIVERSITY OF GENOVA

PHD PROGRAM IN BIOENGINEERING AND ROBOTICS

Diffusion studies of nanomedicines within increasing complexity tissue models

Valeria Lusi

Thesis submitted for the degree of Doctor of Philosophy (32° cycle)

December 2019

Paolo Decuzzi — Supervisor

Giorgio Cannata — Head of the PhD program

Dibris

Department of Informatics, Bioengineering, Robotics and System Engineering

Acknowledgements

This project was partially supported by the European Research Council, under the European Union's Seventh Framework Programme (FP7/2007-2013)/ERC grant agreement no. 616695, by the Italian Association for Cancer Research (AIRC) under the individual investigator grant no. 17664, and by the European Union's Horizon 2020 research and innovation programme under the Marie Sklodowska-Curie grant agreement no. 754490. I would like to acknowledge the Nikon Center, the animal facility and the electronical microscopy facility in IIT as well as the Galliera Hospital and Politecnico di Milano too for the collaboration at this work.

Abstract

Many solid tumors develop biological characteristics different from those which characterize the healthy tissues; compared to normal tissues, tumoral main features include blood vessels with fenestration and a higher rigidity of extracellular matrix (ECM) that, with its architecture, influence drug delivery and diffusion to the tumoral mass [1] [2] playing a leading role on the effectiveness of the therapy [3].

Living cells are always surrounded by extracellular matrix, which can be understood as a three-dimensional structured filter; no substance can pass directly from the bloodstream to cell and vice versa, but must reach the cell over the ECM.

The nanocarriers are the most important drug transporters to whom the researchers always pose attention for overcoming biological barriers to enabling the drug reach the pathological site. They can carry hydrophilic and/or hydrophobic drugs, protecting them from degradation, providing a drug controlled release and reducing toxic effects to the healthy tissues [4]. Particles movement in tissues depends on their size, charge, and configuration and these features can be modified in order to optimize particles delivery to cancer cells. As well as from particle features, particle movements depend also on ECM properties; it is necessary to understand the best way how these particles diffuse in the ECM [5].

Drug and particles transport through interstitial tissue is ruled by a diffusive flux due to concentration gradient and a convective flux due to fluid movement even if high interstitial fluid pressure makes the transport of drugs dependent only by the diffusion [3]. Drug delivery depends also on the cells that form the tumor mass and on the matrix

structure [6]. It is of fundamental importance to understand how these barriers interfere with the drugs transport to improve even more the transport of therapeutic molecules [3].

For this purpose, in this work it has been developed a Tissue Chamber Chip that represents a tool to investigate the diffusion of different nanoparticles (NPs) in an extravascular space modeled by collagen, the main component of the extracellular matrix.

Before clinical trials and food and drug administration (FDA) approval, drugs and delivery mechanisms need to be tested to determine their effectiveness and toxicity. Here, six different nanocarriers, almost similar in size but with different surface decoration were tested. The found results highlight that the surface PEGylation promotes diffusion by acting as a lubricant agent. In particular, it has been found that the greater the percentage of PEG on the surface, the greater the mobility of these nanovectors within the ECM. The particles covered with hyaluronic acid, instead, showed a different behavior: their diffusion was hampered proportionally to the molecular weight of this glycosaminoglycan.

To demonstrate the generality of our approach, the same NPs were tested on murine brain tissue. The results obtained provide the same trend that can be seen from collagen alone, even if the order of magnitude of the diffusivity is different because of the tissue architecture and complexity.

Collectively, these results suggest that the procedure adopted for the nanomedicine diffusion studies, regardless of the tissue, is solid. And, in particular, this suggests that the Tissue Chamber chip can be used as a predictive model of NPs behavior within a biological environment.

Finally, to further increase the translational characteristic of our platform, the same collagen matrix was used as a nutritional environment for a 3D culture of cells derived from colorectal cancer. The *in vivo* tumor tissue has been recreated *in vitro* in order to potentially allow patient-specific drug screening and the development of personalized treatment [7].

This work demonstrated that our device can be efficiently used to test the extravascular transport of NPs and, moreover, it can be modified increasing its complexity to get closer to a real model.

In addition, this project could continue using patient-derived 3D culture to effectively test drugs and NPs to make clinical trials increasingly oriented and well targeted.

Table of Contents

List of figures

Chapter 1

1. Introduction

1.1 Nanoparticles in Medicine

Current treatments in oncology include surgery, radiation therapy and the use of chemotherapy drugs that often kill healthy cells and cause toxicity to patients; therefore, it is desirable to develop chemotherapy that can be passively or actively addressed to cancer cells. Nanotechnology has the potential to revolutionize cancer diagnosis and therapy but, so far, only few drugs nanocarriers have been clinically approved [8].

An ideal anti-cancer drug should reach the tumor without systemic loss, penetrating the tumor mass, and completely eradicate the tumors. Frequently the effect of an anti-cancer drug is limited to the tumor vasculature periphery so that the central part of the tumor mass is not reached by the drug and becomes a source for the relapse of the tumor or metastases. Because of their size compatible with cellular and subcellular functionality, over a wide superficial area than could be modified, nanoparticles have been elected as promising vehicles for drug delivery of anti-cancer drugs. Protecting the nanometric particles with a suitable surface coating, these ones may circulate for a prolonged time. They can also accumulate in a solid tumor through full of fenestrations vasculature that increase the drug delivery to the tumor. But, because of the considerably larger dimension than free molecule, nanoparticles might find obstacles in the penetration of the tumor

mass. This suggests that drug nanocarriers effectiveness may be limited if they are designed without taking into account the physiological barriers [1].

Nanotechnology that arise from the collaboration of engineering, biology, physics, chemistry and medicine has produced devices such as nanocarriers for delivery anticancer drugs, and contrast agents for imaging. The classic definition of nanotechnology devices requires that the device itself or its essential components have nanometric size (diameter 1-100 nm) in at least one dimension [1]. Examples of nanotechnology devices in medicine include nanocarriers for drug delivery or implantable platforms. Nanocarriers injectable in an intravascular way, are the main class of nanotechnology devices of interest for use in oncology [9].

Passive targeting represents the basis of clinical therapy; its specific preferential accumulation of therapeutic agents in target tissues is due to biological and structural cancer features. Because of higher metabolic demand, cancer cells need new blood vessels near tumors to provide oxygen and nutrients. This leads to tumor vessels with numerous fenestrations caused by enlarged gap junctions between endothelial cells. Nanocarriers can passively reach the tumor site and accumulate selectively in the tumor thanks to this characteristic known with the name of enhanced permeability and retention effect (EPR) [10].

Through this effect, particles smaller than 200 nm can passively reach the tumor [9].

Nanocarriers for passive targeting have reached clinical trials in the mid-1980s; ten years later, the first product based on liposomes and polymer-protein conjugates [8] was commercialized [8]. Passive targeting with nanocarriers suffering certain restrictions since the particles, during their path, encounter physiological barriers like mucosal, non-

specific absorption and non-specific drugs delivery that make it hard to control the process; moreover, sometimes target cells within a tumor are not always feasible because of ineffective diffusion of some drugs. Other examples of the hurdles that a nanoparticle, a therapeutic agent or free imaging agent has to face during its way to the target site are the blood brain barrier, vascular endothelium as well as the increased osmotic pressure within the tumor mass that causes the expulsion of the carrier; these therapeutics could also be seized by the reticuloendothelial (RES) [9]. Passive targeting is also limited because some tumors do not exhibit the EPR effect, and vessels permeability may not be the same in each part of a single tumor. Engineering the nanocarriers binding, through the most appropriate chemical bonds, on their surface target agents such as a ligand or an antibody, allows these carriers to link actively specific cells after extravasation through a ligand-receptor mechanism. The nanocarriers are internalized and then the drug is released into the cell; this is a strategy to overcome the limitations of passive targeting and this mechanisms is known as active targeting [10]. In general, when using a targeting agent for nanocarriers delivery to cancerous cells, it is necessary that the agent selectively binds to overexpressed molecules on the surface of target cells compared to normal cells. It is known that a high binding affinity reflects an effective targeting but, on the other hand, especially with solid tumors, this high affinity may create a protective barrier to the penetration of the drug within the tumor mass by limiting the therapeutic effectiveness only to the outer layer. Since free drugs in the blood stream have a poor stability and therefore a limited shelf-life, the idea of using drug nanocarriers that can protect a payload drug from degradation has gained ground, as well as the possibility to administrate intravenously not only hydrophilic drugs, but also hydrophobic ones providing a hydrophilic coating of the particle [9].

Nanocarriers used instead of free drugs has additional benefits:

- Encapsulating a drug in nanocarriers, not only protects it from premature degradation but also from premature interaction with the biological environment,
- It increases the absorption of drugs in target tissues,
- Pharmacokinetics and drug distribution profile in the tissue can be controlled
- Cell penetration is improved as well as toxicity to healthy tissues is decreased and the drug can reach the lesion site without systemic losses. The nanocarriers, in fact, can also be used to increase the local concentration of the drug carrying it inside the target cell and control its release when bound to targets.

Another advantage in using nanotechnology in medicine is the possibility to be able to load within these carriers a combination of drugs or a chemotherapeutic agent and an imaging one to realize the so called theranostics: contemporary diagnostic imaging and therapy [11].

Another important feature of the drug delivery systems is the ability to modulate the drug release making sure that this is slow and prolonged in time. Having systems that selectively target diseased cells means avoiding to the patient side effects caused by the drug on healthy tissue; with a free drug, large doses should be used so that effective concentrations arrive at the site of the lesion. Nanomedicine can avoid this problem by loading in the nanoparticles a proper amount of drug avoiding or decreasing serious side effects due to free chemotherapeutic drugs.

In order for the nanocarriers designed and engineered in the laboratory to be quickly used in the clinic effectively, the nanocarriers should:

- Be made of a biocompatible material, well characterized and easily functionalized;
- Exhibit a high differential absorption efficiency in target cells compared to cells or normal tissues;
- Not be toxic;
- Show stability in the tumor microenvironment;
- Be soluble in aqueous solution;
- Have an increased circulating half-life, low aggregation rate, and a long life.

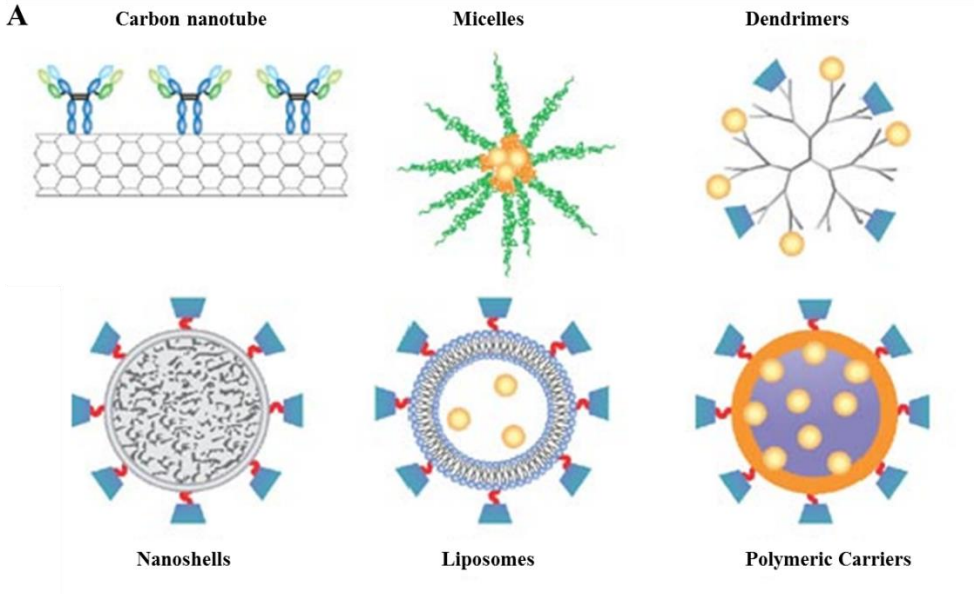

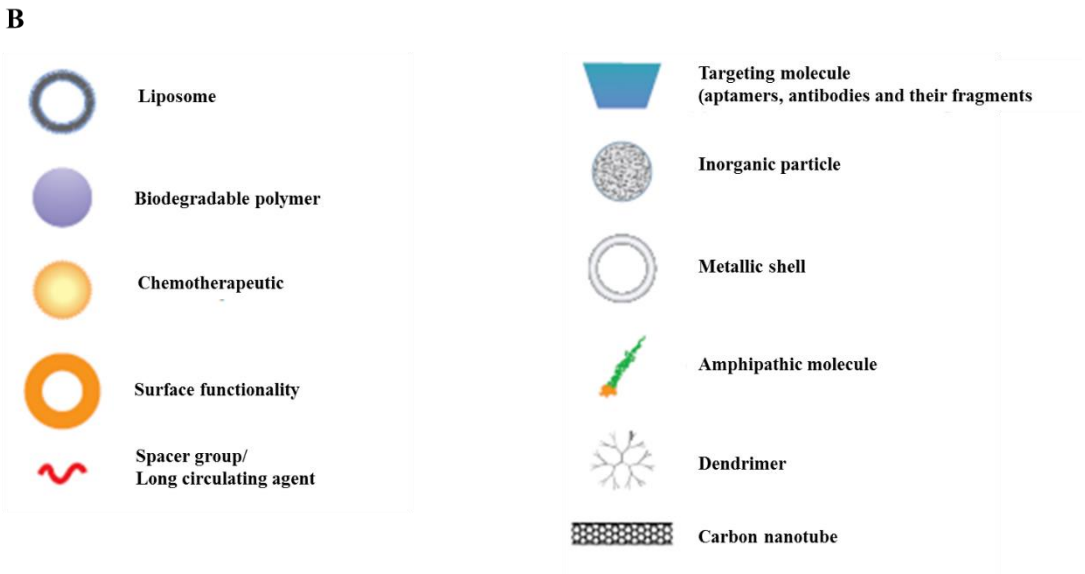

Figure 1.1 *A. Nanovectors models and B. Nanovectors details [8]*

The nanocarriers are generally made up by a material constituting the core, a drug and / or an imaging agent loaded, and a ligand of the surface [9]; these vectors are not only studied for drug delivery but also for imaging and thermal ablation of cancer. Their ratio surface area / volume is so great that it is possible to achieve high density of ligands on the surface so that, currently, there are already clinical formulations of approved carriers for drug delivery made from natural and synthetic polymers and lipids.

The various types of nanocarriers are presented in the **Figure 1.1** and are:

- Carbon nanotubes;
- Carrier based on lipids such as liposomes and micelle;
- Dendrimers;
- Nanoshells;
- Polymeric carriers.

The polymers are the most commonly studied materials for nanocarriers structure. For the realization of polymeric nanoparticles, synthetic polymers may be used for example poly (lactic acid) (PLA) and poly (lactic co-glycolic acid), or natural polymers such as chitosan and collagen.

Polymeric particles may be directly synthesized with a drug inside and their surface can be functionalized with a ligand or a therapeutic agent.

Drugs can be released according to various strategies:

- In a controlled manner through the bulk or surface erosion;
- Diffusion through the polymer matrix;
- Release following a response to the local environment.

In addition to polymers, as base material for the realization of nanocarriers, lipids were also investigated. Lipid based nanocarriers are biocompatible, biodegradable, they isolate the drug from the surrounding environment and are able to entrap both hydrophilic and hydrophobic drugs. Adding agents to the lipid membrane and modifying the surface, properties of these carriers such as the size, charge and surface functionality can be appropriately modified.

Liposomes are self-closed spherical structures formed by one or more concentric lipid bilayers with an aqueous phase inside. Within the aqueous phase it is possible to entrap a polar molecule while inside the lipid bilayer it is possible to trap a hydrophobic molecule. To increase their circulation half-life, liposomes may be coated with PEG that could increase by 10 times the liposomes circulation half-life. Today liposomes are approved by the regulatory agencies to bring a range of chemotherapy.

Liposomes are the simplest form of nanocarriers; the formulation of doxorubicin encapsulated in liposomes was approved in 1995 for the treatment of Kaposi's sarcoma and now is used against breast cancer and refractory ovarian cancer. Liposomes continue to be refined and applied to multiple cancer indications [9].

Polimersomes have architecture similar to that of liposomes but they are composed by amphiphilic synthetic polymers, including copolymers of (polylactic acid) PLA-based.

Micelles, which are self-assembling monolayers closed with a hydrophobic core and a hydrophilic shell, have been successfully used as pharmaceutical carriers for insoluble drug in water. They belong to a group of amphiphilic colloids which can be formed spontaneously under certain conditions and temperatures from amphiphilic or surfactants agent. The hydrophobic drug is inside, protected from the hydrophobic core; the external hydrophilic shell allows the stability of the encapsulated drug in a physiological environment.

Dendrimers are synthetic branched macromolecules that form a branched-structure. Dendrimers have highly branched macromolecules, composed of several extremely branched monomers that emerge radially from the central core. The modifiable surface characteristics of dendrimers enable them to be simultaneously conjugated with several molecules such as imaging contrast agents, ligands or therapeutic drugs, and hence have created a multifunctional drug delivery system [10].

The inorganic particles are based primarily on metals. The inorganic materials have been studied extensively for magnetic resonance imaging. Specific types of newly developed inorganic particles, include Nanoshells and gold particles. Nanoshells (100-200 nm) are

composed of a silicon core and an outer metallic layer and may use the same carrier for the imaging and therapy.

The choice of an appropriate nanocarrier is not obvious therefore; successful targeting strategies have to be determined experimentally case by case in a laborious way.

Since approximately the turn of the millennium, nanoparticles have been promoted as a paradigm-shifting approach to early diagnosis and improved treatment of multiple diseases [9] [12]. The potential of particle-based drug delivery systems, or in a simple word nanomedicines, to protect drugs (small molecules, biologicals, peptides, etc.) from premature degradation, prolong the circulation time in the blood, reduce systemic toxicity, and control release has been documented extensively by the scientific community [13]. Moreover, nanomedicines enabled the realization of multifunctional delivery systems with combined therapy and diagnostics (e.g. theranostics) [14] [15] [16], co-delivery of drugs [17] [18], and targeted delivery [19] [20].

Although several nanomedicines, mostly lipid-based formulations, are under clinical investigation in early and advanced trials, there are still significant challenges in fully integrating nanomedicines into clinical practice. Some of these challenges are merely technical, such as the difficulty in the reproducible synthesis and large-scale manufacturing [13], while others are due to challenges in fundamental understanding of particle behavior in complex biological systems [21] [22]. To this last point, a major interest in nanomedicine is understanding the transport of particles across biological barriers to their final pathological targets and critical to this goal is understanding the dynamics of particles through the extravascular tissue [23]. Researchers have attempted to overcome this grand challenge by tailoring particle physico-chemical properties (i.e.

size, surface charge, surface functionalization, material density, shape, etc.), utilizing stimuli-responsive materials, masking particles in cellular coatings, using cells to shuttle particles across barriers, or employing multi-stage delivery systems. For example, Cabral et al. [24] showed in vivo that particle size (30 to 100 nm) played a significant role in the accumulation of nanoparticles in tumors of varying permeability. That is, size had little effect on particle-tumor accumulation in highly permeable tumors, however when tumors have low permeability the smaller particles (30 nm) accumulate more compared to medium-sized (50 nm) or larger particles (70 and 100 nm). One approach to capitalize on these phenomena is to develop particles that modulate their size throughout their voyage to the target site. Wong, et al. [25] reported multistage nanoparticles that shrink from approximately 100 nm in diameter to 10 nm as they extravasate from the tumor vasculature into the tumor tissue. This was achieved by having a primary particle that can be actively degraded by proteases in the tumor microenvironment, thereby releasing smaller non-degraded particles (i.e. 10 nm quantum dots). In this case, the larger primary particles enable long circulation half-life and passive tumor targeting, and the release of small particles enables deeper tumor penetration. Another such multistage particle system was reported by Tasciotti et al. [26], where larger, mesoporous silicon primary microparticles were loaded with quantum dots or single-walled carbon nanotubes (SWCNTs). This system takes advantage of the micron-sized and specifically shaped primary particles' ability to marginate in the vasculature to better deliver the nano-sized quantum dots or SWCNTs. Finally, biomimetic approaches are attempting to utilize naturally occurring cellular processes to transport particles across biological barriers. Particles have been coated in "stealth" cellular membranes to avoid immunological detection and clearance, and improve tumor targeting [27] [28]. Furthermore, particles

have been attached to cells as “hitchhikers” [29] [30] or transported across biological barriers as intracellular cargo [31] [32] [33]. Despite all of these innovative approaches to optimize particle transport across biological barriers, there exists a need to understand particle transport through tissues on a fundamental level.

Only few systems have been approved by the food and drug administration (FDA): one of these is Doxil that represents liposomal formulation of doxorubicin and one is the Abraxane which is based on the nanoparticle albumin bound (nab) technology to deliver paclitaxel, a drug largely used for breast and pancreatic cancer. The slowness of the translation process from the bench to the patient’s side can be attributed to many issues, the most critical is the loss of relevant platforms for preclinical tissue culture that can mimic in vivo conditions and predict the behavior of these nanoparticles within the human body [34].

1.2 Barriers to drug transport

The extracellular matrix is the most complex structural organization units of tissues in living organisms. Tissues do not consist only of cells but a large part of their volume is formed by extracellular space, filled by an intricate network of macromolecules whose three-dimensional organization is the ECM. It is composed by many proteins and polysaccharides that join together in a network organized compactly and connected to the surface of cells that produced it and to surrounding ones. ECM isn't only the relatively inert scaffold able to stabilize the physical structure of the tissues but it is also the substrate on which all the tissues cells may adhere, migrate, proliferate and differentiate, and which influence their survival, shape and function. The ECM macromolecules, in fact, seize growth factors, molecules such as water or minerals and controlling physiological pathophysiological and pathological phenomena, such as morphogenesis, wound healing and tumor invasion and metastasis. Many solid tumors develop biological characteristics different from those which characterize the healthy tissues; compared to normal tissues, tumoral main features include blood vessels with fenestrations and a higher rigidity of extracellular matrix (ECM) that, with its architecture, influence drug delivery and diffusion to the tumoral mass laying a leading role on the effectiveness of the therapy [2].

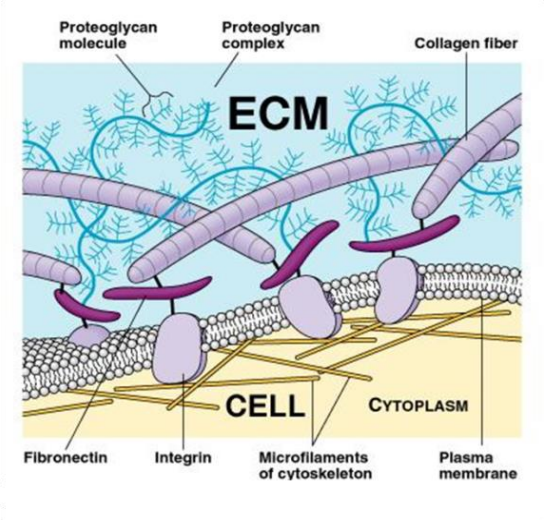

Figure 1.2 *Extracellular matrix architecture (Adapted from 1999 Addison Wesley Longman. Inc.)*

The Extracellular Matrix (**Figure 1.2**) is made up of a large variety of macromolecules and its composition varies from tissue to tissue even though it is made up from the same basic elements. The characteristics of these molecules associated with the specific-tissue ECM as well as the way in which they bind to each other and to the ECM structure, determine resulting ECM structure and organization. It is specifically adapted to facilitate the functional demand of the tissue from which it originates due to the specific architecture characteristics and composition [35]. The main components of the ECMs are structural proteins such as collagens (that gives strength to the structure), laminins (that gives flexibility), glycoproteins, proteoglycans (PGs) that are the most important structural and functional macromolecules in tissues, and glycosaminoglycans (GAGs) where hyaluronic acid is a linear GAG [36].

Living cells are always surrounded by extracellular matrix. Collagen, proteoglycans and hyaluronic acid are the primary structural components in the ECM; they provide support for the other components of the ECM and for cells interacting within the structural

network. Other components of the ECM, like laminin or fibronectin act as bridges between the structural molecules of the ECM to strengthen it, as well as to connect the ECM to the cells and molecules of the extracellular space. The collagen and the elastin are a part of fibrous proteins class; proteoglycans, fibronectin and laminin are part of the glycoprotein ones [35].

Each class of ECM molecules interacts with another class to create unique physical and signal properties that support the tissue structure, its growth and its function.

Collagen (**Figure 1.3**) is the mainly present proteic component in the ECM. Despite the existence of different types of collagen, the item that they share is the triple helix structure made of three polypeptide chains.

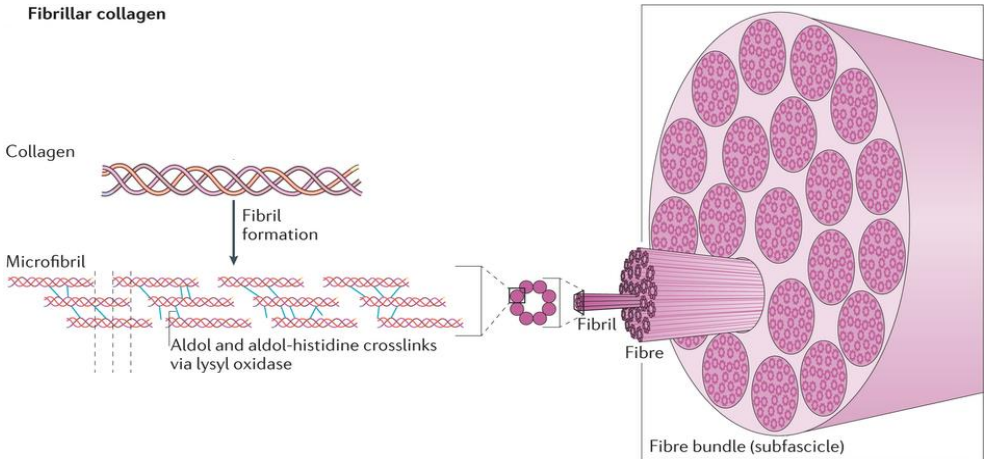

Figure 1.3 *Collagen fibers representation (Adapted from extracellular matrix assembly: a multiscale deconstruction)*

Proteoglycans (**Figure 1.4**) perform their primary biological function due to biochemical and hydrodynamic glycosaminoglycans (GAGs) characteristics present in the molecules; GAGs are linear chains of disaccharides characteristically long and negatively charged. These compounds bind water in order to proceed to hydration and compressive strength. Proteoglycans are characterized by a core protein covalently bound to GAGs.

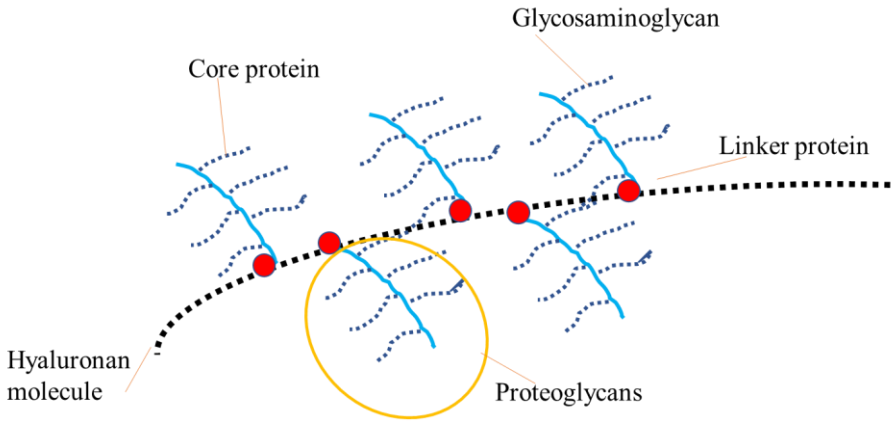

Figure 1.4 *Proteoglycans structure.*

Laminins (**Figure 1.5**) are large glycoproteins that mediate interactions between cells via cell surface receptors (such as integrins) and other ECM components through modular domains within the laminin molecule. They are located mainly in the basal lamina and in some mesenchymal compartments.

The Fibronectin (**Figure 1.5**) is a large fibrous glycoprotein with the role of binding cells to the ECM. Each subunit of fibronectin consists of three modules of repeating units, each of which has an important structure to facilitate fibronectin interaction with cell surface receptors. A significant part of ECM proteins, interact with cells via connections with the fibronectin to regulate cell adhesion, as well as migration.

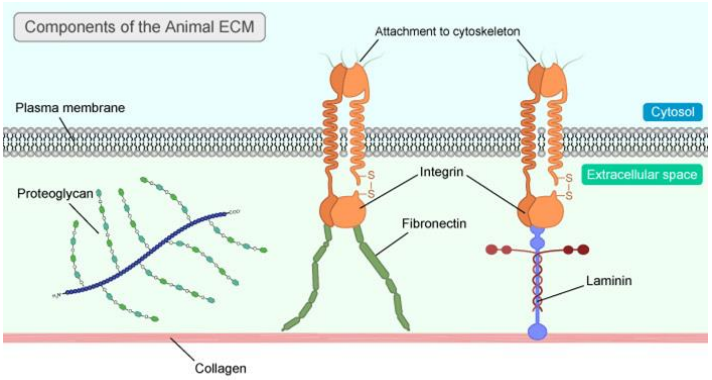

Figure 1.5 *Fibronectin and laminin representation (Adapted from Rose L. Hamm: Text and atlas of wound diagnosis treatment)*

The properties of the ECM are altered in many diseases either as a cause or as a result of the disease pathogenesis. For example, old and sick tissues are often more fibrotic presenting the classical components of the ECM at higher concentrations or organized in an inadequate way, causing a mechanical impairment of tissues. Components at higher concentration than that found in a normal ECM are present in the tumor extracellular matrix including collagen type I, II, III, V and IX. Even the architecture of proteins secreted in the ECM is altered in cancerous tissues in fact, the increased collagen density and its abnormal organization, promotes the development of cancer and metastasis as well as the recurrence after surgical resection [37].

Before clinical trials and Food and Drug Administration (FDA) approval, drugs and delivery mechanisms need to be tested to determine their effectiveness and toxicity. The first step in this process begins with in vitro testing of the drugs and their delivery methods. Typically these delivering tests are performed in 2D cell cultures: the majority of cell-based assays use 2D monolayer cells cultures despite they have increasingly recognized limitations [38]. They slightly mimic the in vivo condition: they don't accurately predict in vivo toxicity and other biological effects because of the absence of

physiological processes such as transport of drugs and Nanoparticles (NPs) through cell layers in contact with the tissues [39]; this can seriously compromise the reliability and significance of data obtained from 2D approaches [40]. Since 3D cell culture reproduce in more truthful way physiological cell-cell contact geometry, mass transport, and tumor mass mechanical properties, they can offer better models for drug delivery toxicity tests than conventional 2D cultures. The most common methods to culturing cells in 3D is the growth of microscale, spherical cell clusters formed by self-assembly: the spheroids [41]. They may be obtained with various techniques designed for aggregation of the cells through the promotion of cell adhesion, avoiding the interaction cell-contact surface [42].

In vivo disease models are the benchmark for studying particle transport processes as they are dynamic, complex, and mimic the biological fate of particles in human biology. However, organs-on-chips technologies are increasingly being looked at as alternatives to animal models [43]. These technologies are developed with increasing complexity (i.e. able to mimic organ and organ systems), while providing precise control over the system engineering and parameters. In fact, previous studies on a simplistic collagen matrix have shown that the ionic strength of media, particle surface charge, and biophysical properties of the matrix heavily influence the diffusivity of quantum dots into a collagen gel [6].

1.3 Diffusion in tumoral extracellular matrix and measure methods

Particles move Brownian random motion within intricate network that constitutes the ECM and they are influenced by this in three different ways.

- Collision with the matrix fibers generating steric interaction;
- Diffusing near the fibers, a limited thermal motion of water molecules slows their motion (hydrodynamic interactions);
- Electrostatic interactions with charged components of the extracellular matrix (for charged particles) [5].

Drugs and particles transport through interstitial tissue is ruled by a diffusive flux due to concentration gradient and a convective flux due to fluid movement even if high interstitial fluid pressure makes the transport of drugs dependent only by the diffusion [3] drug delivery depends also on the cells that form the tumor mass and on the matrix structure [6]. Diffusive transport of nanoparticles and/or macromolecules in a charged fibrous media is an interesting field in drug delivery; experimental findings have shown that diffusion may be significantly hindered by electrostatic interactions between diffusing particles and charged ECM components [6]. Since diffusion of therapeutic agents in ECM plays a fundamental role in reaching lesion sites, it is essential to understand how these barriers interfere with the transport of the drugs to improve even more the transport of therapeutic molecules [3]. The continuing progress of nanotechnology has led to develop particles with controllable size and surface charge and with the potential of being used for cancer detection and treatment. Studies on the hydrodynamic interactions effect of the nanoparticles diffusion in fibrous media have

shown that the effective particles diffusivity within the ECM may also decrease by three orders of magnitude because the particles bind to the surface of ECM fibers [6]. Tracing the trajectory of the particles for 10,000 time steps and taking the average over the 1000 particles, the local diffusion coefficient D, and the components of the main diagonal of the tensor of the global diffusion coefficient (D * xx, D yy *, D * zz) is so determined [6] :

$$D = \frac{< MSD >}{6t}; \quad D^*_{xx} = \frac{< MSD_x >}{2t}; D^*_{yy} = \frac{< MSD_y >}{2t}; D^*_{zz} = \frac{< MSD_z >}{2t}$$

Where t is the time and the mean-square displacements(MSD) were calculated from:

$$< MSD > = \frac{1}{n}\sum_{i=1}^{n}\left[\left(x_i(t) - x_i(0)\right)^2 + \left(y_i(t) - y_i(0)\right)^2 + \left(z_i(t) - z_i(0)\right)^2\right]$$

$$< MSD_x > = \frac{1}{n}\sum_{i=1}^{n}\left(x_i(t) - x_i(0)\right)^2$$

$$< MSD_y > = \frac{1}{n}\sum_{i=1}^{n}\left(y_i(t) - y_i(0)\right)^2$$

$$< MSD_z > = \frac{1}{n}\sum_{i=1}^{n}\left(z_i(t) - z_i(0)\right)^2$$

Where n is the total number of particles and x_i, y_i, z_i are the coordinates of the direction of the particle i.

These models can be used in a much more reliable way as the hydrodynamic diameter of the diffusing molecule (or nanoparticle) is small compared to the diameter of the fiber; otherwise, the diffusivity is affected by hydrodynamic interactions [44].

It is known that positively charged particles are able to selectively target tumor vessels but the authors showed that neutral particles may diffuse faster than cationic ones since the tumor ECM consists of positively charged collagen fibers and hyaluronic acid negatively charged.

Therefore, it is concluded that the optimal nanoparticle for delivery to tumor tissues should be initially cationic in order to selectively target tumor vessels but should change charge and become neutral after entering into ECM [6].

As an alternative, to completely remove any convective component from the measurements, the Fluorescence Recovery After Photobleaching (FRAP) technique could also be used [45].

FRAP, known also as (micro) photolysis is an optical technique, based on optical microscopy, used to quantify the diffusion of fluorescently labeled probes in a sample. Fluorescent emission depends upon absorption of a specific optical wavelength that restricts the choice of lamps.

Next, the light source is focused onto a small spot of the viewable area where fluorophores receive high intensity illumination that causes their fluorescence lifetime to quickly elapse.

As Brownian motion proceeds, the still-fluorescing probes will diffuse throughout the sample and replace the non-fluorescent probes in the bleached region. This diffusion proceeds in an analytically determinable way from the diffusion equation.

Fluorescent molecules diffusion coefficient (D) can be derived from the recovery of fluorescence in the bleached area [46].

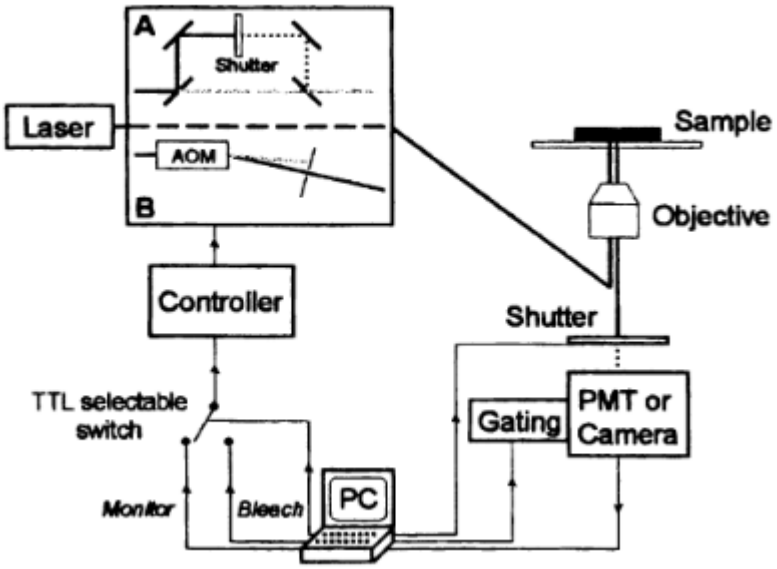

Figure 1.6 *FRAP setup [46]*

In **Figure 1.6** it can be seen the most recent setup illustrating two possible setups intensity modulation of the light. There is a light source with a bleaching power and a light to monitor the fluorescence before and during the recovery process of fluorescence. Typically, an intense laser light is used for bleaching and for monitoring, a laser light or a light from a mercury vapor lamp is used. Choosing to use a laser light, one single laser source is used for both the bleaching and the monitoring. Other instruments use a dual beam splitter which divides the laser beam into a beam of high and low intensity; those will then be assembled before the entrance to microscope. A faster system can be obtained using an acousto optical modulator (AOM) which has a response time of a few microseconds. All these optical modules can be installed in conventional fluorescent microscopes or in a confocal one. The last allows the detection of fluorescence not only on the surface of the sample but also in depth within the sample, without any interference

from the fluorescence of the sample out of focus levels. The FRAP technique was developed to study the mobility of the molecules in biological samples but in time, it was also implemented in diffusion study inside polymer solutions and gels. The fluorescence intensity during the recovery is recorded directly from a signal photomultiplier (PMT) or from the analysis of the images taken during the recovery. The main bleach geometries include circular spots with a Gaussian intensity profile, or uniform after the bleaching or strips. The last ones can be evaluated in the identification of an anisotropic diffusion by changing the orientation of the strips when the experiment is repeated. With a Gaussian intensity profile, the intensity profile after the bleaching must be determined in order to extract the' half width '(ω) necessary to calculate the diffusion coefficient.

The setup in **Figure 1.6** uses a single laser source like excitation and bleaching source; there are two possible intensity modulation setups represented. The upper part, A, is a dual beam-splitter with a shutter; the setup B uses an AOM to diffract the light. Both systems are driven by a controller that translate the signals from a PC in a proper voltage for the AOM or a signal controlling shutter movement. The laser beam is directed into the microscope and towards the sample. The fluorescence is detected by the photomultiplier.

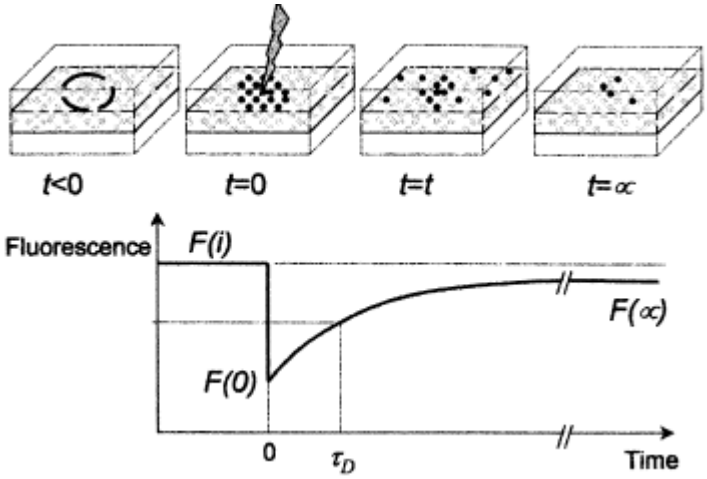

Figure 1.7 *FRAP experiment graph [46]*

Figure 1.7 represents a FRAP experiment scheme. Before bleaching, the monitoring light beam is focused inside the sample and the fluorescence is measured in a proper region of interest (ROI); in this figure there is a circular ROI. The starting fluorescence, before the bleaching process, is named F(i). At zero time, a high intensity light beam bleaches the molecules in an observed area resulting in a fluorescence falling from F(i) to F (0). Due to random diffusive movement, bleached molecules will change their positions in the bleached area with surrounding non- bleached fluorescent molecules. This brings to observe a fluorescence recovery. The diffusion characteristic time (τ_D) is the time in correspondence of which, half of fluorescence has recovered. At the end of the experiment ($t=\infty$) fluorescence has recovered to F (∞), equal to F(i) if all the fluorescence molecules in the observed area are mobile or less than F(i), if a part of fluorescent molecules are fixed in the observed area during the experiment.

A

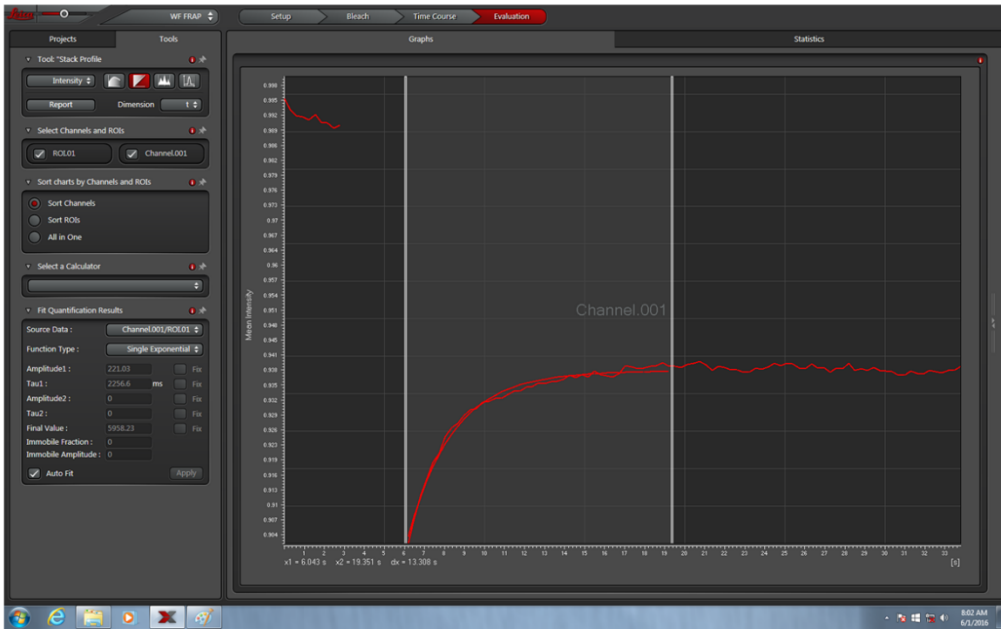

B

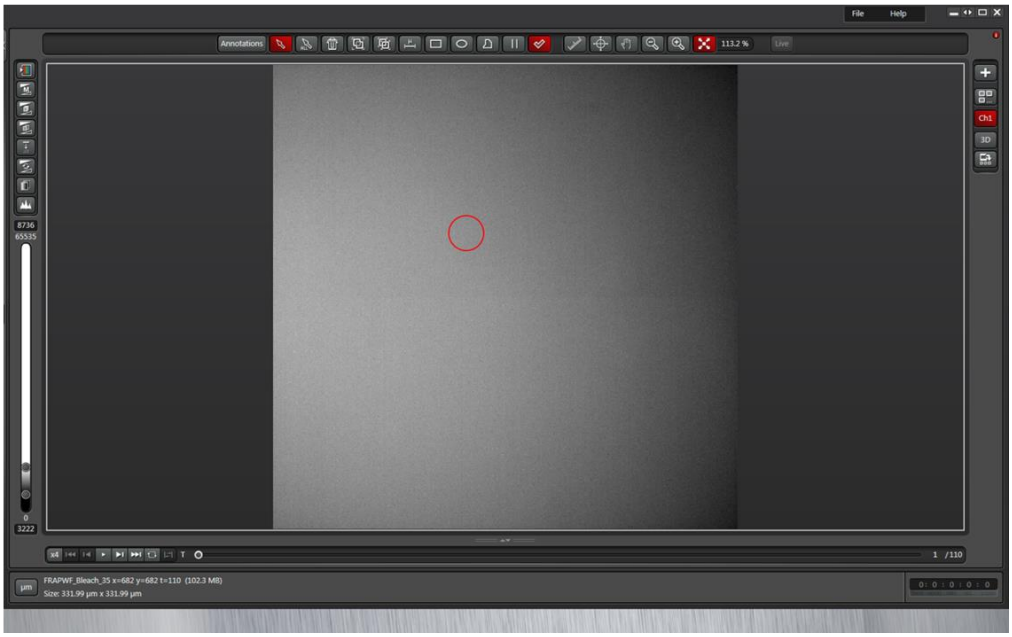

Figure 1.8 *A. Example of a FRAP experiment graph applied to a collagen gel injected with FITC-dextran; B. circular ROI*

Using the confocal microscope, whose operating principle is described in **Figure 1.10**, the FRAP analysis was carried out and, if in **figure 1.7** the FRAP experimental scheme is represented, **Figure 1.8** shows the outcome of a real FRAP experiment carried out for FITC-dextran previously injected in a collagen gel. In **Figure 1.8 B** is well visible the ROI chosen as a region to address the bleaching light. **Figure 1.8 A**, instead, shows the recovery after photobleaching curve as a function of the time. After an optimized and standardized time, the software detects a time value (τ_D) needed for the obtainment of the diffusion coefficient of the particular dye.

Axelrod et al. developed a method to analyze the FRAP data and obtain a quantification of molecular mobility and interactions. Still many FRAP analysis are based on Axelrod's equations [46].

Axelrod's theory is based on some fundamental assumptions:

- There must be no flow then the recovery of the fluorescence must be the result of pure diffusion in two dimensions in an infinite plane; therefore, it must derive from the diffusion of molecules within the same bleached floor area;
- During the bleaching there should not be diffusion into and outside the bleached area.

Respecting these conditions, the recovery of the fluorescence in a circular bleached area, with a fluorescence intensity Gaussian profile, can be described by the normalized fluorescence recovery curves (f (t)):

$$f(t) = \sum_{n=0}^{n=\infty} \frac{-\kappa^n}{n!} * \frac{1}{1 + n\left[1 + \left(\frac{2t}{\tau_D}\right)\right]}$$

Where κ is the bleach constant, that measures the amount of fluorescent molecules that have been bleached;

τ_D is the characteristic diffusion time related to the diffusion coefficient through the following formula:

$$\tau_D = \frac{\omega^2}{4D}$$

Where ω is defined as half of the width of the Gaussian intensity profile of the laser spot and determined to 2-times the height of the profile, and D is the diffusion coefficient [46].

The choice of the fluorophore for FRAP experiments depends on the present excitation source, by the hydrophilic or hydrophobic properties of the medium in which the fluorophore needs to be dissolved, but also the mode that has been chosen to attach it to the particle surface.

Moreover, this choice is a compromise between the fluorophore photostability and its instability.

An easily bleachable molecule has the advantage of being able to be bleached using low bleaching intensity, but it also has the disadvantage of increased sensitivity to the bleaching during the fluorescence recovery process. Fluorescein isothiocyanate (FITC) is the hydrophilic fluorophore most commonly used because it can be easily linked to proteins and polysaccharides and it has a good balance between photostability and instability [46].

Another microscopy technique to calculate the molecular diffusion in the tissues is the Fluorescence Correlation Spectroscopy (FCS). This technique allows the measurement of

diffusion coefficients and concentrations for fluorescing molecules; it is usually run on a confocal microscope and it could be applied to any fluorescently labeled molecules in water or buffer solution, on membranes and also in living cells. The determination of parameters connected to molecules movement represents one of the main FCS analysis objectives in aqueous solution. Its sub-micrometer spatial resolution makes FCS a suitable technique for intracellular measurements [47] .Then researchers want to understand how a biological process works in detail, it is important to distinguish between diffusion, active transport or convection. FRAP technique was preferred to FCS for long time for in vivo motility studies since FCS gives background suppression and undesired photobleaching problems although it determines diffusion coefficients within tens of seconds and with brilliant statistics. Compared with fluorescence recovery after photobleaching, FCS uses lower dye concentrations and laser powers reducing the perturbation to the biological system; it has also an increased sensitivity [48].

The last technique could be used to measure the diffusion coefficient D since it contains informations about the size and weight of the moving particle. D describes how far a particle may go due to its concentration gradient but diffusion can also be described as a random walk in the solution in fact, while a protein moves in water, the water molecules colliding with them cause their walking in random directions. This leads to a random trajectory r(t) of the individual molecule. The trajectory could be analyzed by mean squared displacement (MSD), $\langle r^2 \rangle$, that represents the area covered by the particle in a definite time. It is linear with the time and the diffusion coefficient is the proportionality coefficient:

$$r^2 = 6\, D\, \tau.$$

Diffusion can be described by Fick's law that is a macroscopic one (that could not be derived from microscopic observations like Brownian motion for example) that defines the diffusion like an equilibration of concentration gradients. Albert Einstein, instead, derived a relation for the diffusion coefficient, by connecting the diffusion coefficient itself with the particles properties and the solution in which they are moving. This relation is the Stokes-Einstein equation:

$$D = k_B T / 6\pi \eta R_h$$

where $k_B = 1{,}3806504 * 10^{-23}$ J/K is Boltzmann's constant, T is the temperature and η is the solutions viscosity.

Fluorescence Correlation Spectroscopy (FCS), derives the sample properties from fluctuations caused by the particles movements. The fluorescence intensity I(t) emitted by the particles is measured: the whole intensity is proportional to the number of particles observed, N.

In FCS overall particle number, N(t), over time is splitted in a mean value <Ni> and small fluctuations dN(t) around <Ni >.

$$N(t) = \langle Ni \rangle + dN(t)$$

Only the fluctuations dN(t) are analyzed; the intensity fluctuations are due to particles leaving and entering the observation volume V_{obs}. If the time that particle spends inside the observation volume is known, its diffusion coefficient, which corresponds to its speed, can be determined. Particles with a large D, show quick fluctuations dN(t), particles with a small D show slower fluctuations. Indeed, in **Figure 1.9**, the fluctuations of two different particles in an observation volume are shown: the red line highlights a slower fluctuation linked to a smaller diffusion coefficient; the opposite is for the blue line. The

correlation analysis done in FCS extracts the characteristic timescale of these fluctuations that can be converted in the diffusion coefficient.

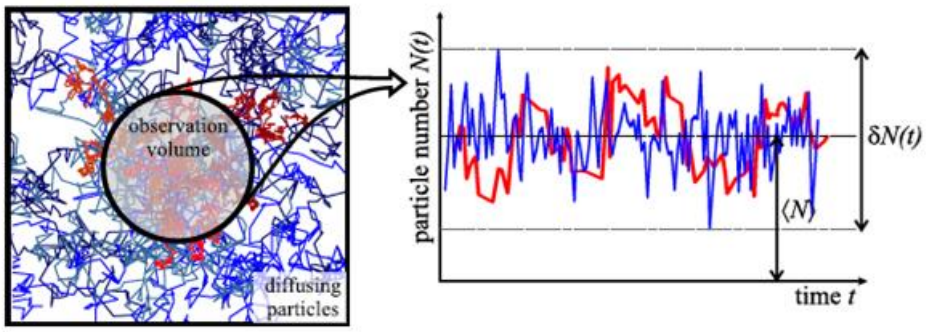

Figure 1.9 *number of particle N(t)=<N> + dN(t) in a specific observation volume for to particles group (blue and red) with different diffusion coefficient (Dblue>Dred). It is visible the different fluctuations timescale dN(t). (Adapted from Imaging fluorescence (cross-) correlation spectroscopy in live cells and organisms. Nat Protoc. 2015)*

FCS is performed using a confocal microscope with high numerical aperture (NA > 0:9) and the focal volume obtained by this setup is on the order of $1fl=1\mu m^3$.

The emitted fluorescence is imaged onto a pinhole that filters the light out of focus and later in a photo-multiplier tube, PMT, or an avalanche photodiode, APD. The APDs produce a pulse for each photon detect and then these pulses can be counted and processed by a computer. A dichroic mirror is used to separate excitation and fluorescence light; an additional dichroic mirror could be used to split the emitted light into several detection channels in order to distinguish different dyes.

The fluctuation is measured by the number of fluorescent molecules that enter and exit from the confocal microscope focus:

$$N(t)=\langle N\rangle + dN(t).$$

Since it isn't possible to directly count the number of the particles, the fluorescence intensity I(t) that particles emit currently inside the focus can be measured, and then, this can be analyzed. While a particle is inside the focus, it is excited by the laser microscope and therefore continuously rounds between its ground and excited state. In each cycle a photon is emitted in a random direction, a fraction of these photons is then collected by the objective lens and afterward detected on a APD that gives rise to an output called I (t).The intensity I(t) fluctuates in the same manner as the number N(t) and each property derived for N (t) is also valid for the I (t) therefore also I (t) can be divided into a constant $\langle I\rangle$ and the fluctuation dI (t): $I(t)= \langle I\rangle + dI(t)$

From this measured signal, it is necessary to extract as fast it fluctuates in order to have information about the speed of the particles in the sample. To do this, a mathematical tool called autocorrelation analysis is used. In FCS, a computer calculates the autocorrelation function g (t) from the intensity signal measured in the microscope I (t). Each FCS measurement produces an autocorrelation curve; to obtain the desired values i.e. diffusion coefficient D and particle number N it is necessary to fit theoretical models to the measured autocorrelation function [49].

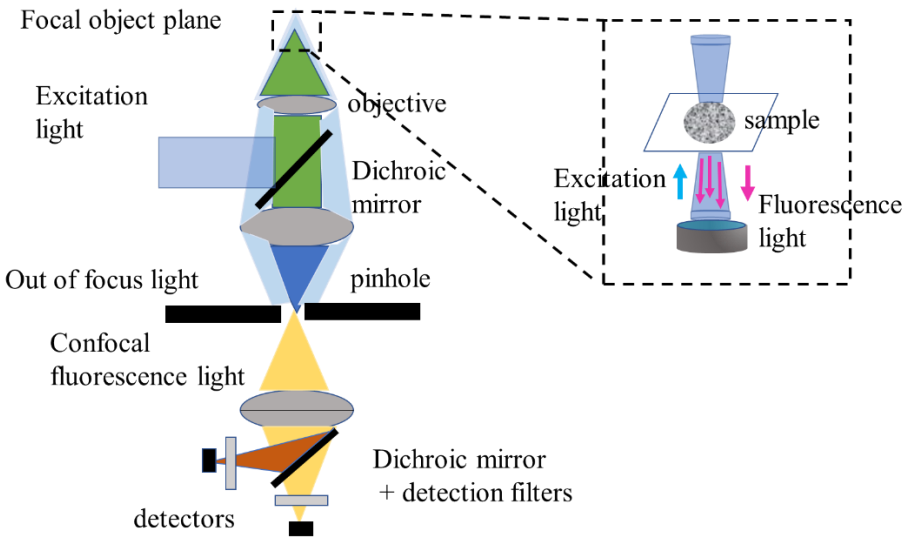

Figure 1.10 *Principle of a confocal microscope*

1.4 In vitro tissue model and organ on a chip

It is increasingly recognized that cancer cells respond differently to anti-tumor drugs when they are surrounded by a three-dimensional extracellular matrix rather than when they are grown in 2D [50]. In vitro tumor models could be applied to in vitro transport studies and cellular uptake of drugs in fact, 3D tumor models are very important tools for studying the diseases mechanisms and for investigating the efficacy of drugs. One of the main advantages of 3D models is that they can allow to study the structural barriers observed in solid tumors which block interstitial penetration and reduce the cellular uptake of drugs. For example, the limited drug delivery into tumor cells was considered to be one of the main causes for an incomplete response of solid tumors to chemotherapy. Most in vitro tumor models are based on spheroids and are used for drug screening. Typically, in vitro developed tumor models are used for in vitro drug delivery studies and drug efficacy studies in a model much more similar to reality. For example, these

spheroids could be combined with fluorescence recovery after photobleaching (FRAP) to study the diffusion coefficient of fluorescent molecules in tumor interstitial spaces. And they can be used to study the penetration of small molecules into tumor tissues [51].

In vitro tumor models have provided important tools for cancer research and serve as an economic screening for drug therapies. However, the recurrence of the cancer remains due to the metastases that are the cause of most cancer-related deaths. Advances in tumor biology, 3D cell culture, tissue engineering, biomaterials and microfluidics have allowed for the rapid development of new in vitro models in which different types of cells are grown, immersed in an extracellular matrix.

The emerging precision medicine has increased interest in the implementation of in vitro tumor models for specific patient therapies as for the assessment of metastatic potential. In vitro models and in vivo animal models are important tools in cancer research for drug screening, for the development of cancer therapies and also to provide information on the molecular mechanisms of tumor growth and metastasis. It is known that in vivo models reproduce the complexity of the disease, while in vitro models have very low physiological relevance, reproducing only limited aspects of the tumor microenvironment. Patient derived tumorgrafts instead reconstruct the heterogeneity of the tumor and in some cases also the morphology of the tumor tissue as well as the genetic expression profile. However, regardless of the cellular source, the models represent an approximation of a tumor and are designed to recapitulate specific aspects of the tumor microenvironment. Although spheroids are more expensive and their management and achievement take longer than 2D cultures, 3D spheroids are more relevantly used for drug screening, tumor growth and proliferation studies and, in the case of spheroids immersed in matrices, studies of invasion and remodeling of the matrix can also be done. These cell

masses also reproduce the interactions between cells and interactions between cells and matrix as well as the interactions between cancer cells and the microenvironment and transport properties. Proteins and the gene expression profile of tumor cells in spheroids are much closer to clinical and in vivo gene expression than those in 2D cultures. If the spheroids are chosen as a tool to mimic the tumor, it must be recognized that there are various methods to obtain them. The suspension culture method, for example, promotes the formation of spheroids keeping the cells in suspension through agitation to allow spontaneous aggregation. The method of culture in suspension is fast but does not allow the control of size and uniformity. Cultivating cells on low attachment surfaces prevents attachment to the substrate and promotes the formation of spheroids as self-assembling. Also, in this case, it is not possible to control the size and uniformity of the spheroids. The use of microfluidic devices and hanging drops techniques allow the control of spheroids size and composition, even if they are more complex. In the case of hanging drop technique, the cell drops are suspended from the underside of an adherent tissue culture lid. Gravity promotes the aggregation of cells in clusters at the bottom of the drop and, then, grow in the form of spheroids. However, whatever the technique chosen, cancer spheroids are widely used to study the response to chemotherapy, target therapy and drug delivery systems. Spheroids can be used both as a tool for negative drug selection to reduce animal testing and for positive selection in new drug development. Choice a spheroid as a drug-screening tool with respect to 2D cultures lies in their greater resistance to treatment and therefore can summarize the drug resistance observed in solid tumors. Drug screening is carried out by incubating the spheroid with a drug and measuring the integrity of the spheroid and the kinetics of growth (for example, delay and subsequent growth) and the size of the surviving cells. There are also other types of in vitro tumor

models including embedded ex vivo tumor section. These models combine the complexity of the tumor microenvironment while maintaining the simplicity of an in vitro model. Embedded ex vivo tumor sections from patient biopsies can be used to select individualized chemotherapeutic treatments and, also in this case, to study tumor growth and invasion; they also can be embedded in an extracellular matrix and can be used to investigate the tumor microenvironment in vitro because they maintain the heterogeneity of the tumor and the tumor vasculature. This technique is widely used for the characterization of tumor morphology and for the tumor mass growth and can also be considered as a technique for the screening of specific patient therapies. Tumor sections are typically embedded in collagen type I as to mimic the ECM although it has been shown that gene expression and phenotypic profiles of cancer cells are dependent on the matrix material. The sections of embedded tissue are largely used for a particular drug sensitivity test (CD-DST) [52] in which the tumor cells obtained from a patient are cultured in collagen droplets and incubated with different chemotherapy; chemosensitivity is evaluated by a number of remaining living cells. Nowadays this technique is in clinical trials for its drug screening feature in patient specific cancer treatment. Moreover, it has been studied and compared with the outcomes of patients with different tumors [53]. The development of 3D culture systems is filling the gap between in vitro and in vivo drug screening methods as well as in vitro 3D models continue to develop to be better indicators of drug efficacy in vivo [53].

New 3D cultures technologies show new scenarios for the development of more physiological models of human cancer. These kinds of preclinical models are very important in order to a more efficient translation of basic research into clinical cancer treatments. Both organoids and spheroids can be obtained from healthy and tumor tissues

derived from patients to test drugs in a specific patient way and in order to identify individualized treatment regimens. Cancer remain the biggest health problem in the world even if the number of deaths related could be reduced through prevention and early diagnosis, as well as with development of new targeted therapies. In order to pursue this scope, there is a need of a model that recapitulates the patient's tumor in order to avoid that working drugs in vitro lost their efficacy in clinical trials. For this purpose, genetically modified mouse models are widely used but they don’t reflect the genetic heterogeneity and complex histology of human tumor tissues. We are therefore looking for more effective models. For example, by incorporating adult stem cells derived from tissue into a 3D matrix, it can be seen that these cells can grow and will be organized in organotypic structures called organoids [54]. This type studies have shown that tumor derived organoid both at the phenotypic and genotypic level resemble the tumor epithelium from which they derive [55]. For example, a collection of patient colorectal cancer cultures was obtained using a method to expand tumor tissues as in vitro tumor spheroids. In addition, during the last years a biobank of tumor organoids derived from 20 genetically different colorectal cancers has been created that match with the organoids obtained from them. The tumor organoids derived from patients, better recapitulate the native tumors and could be major models to identify and test new chemotherapeutic agents. Furthermore, patient derived organoid models of metastatic gastrointestinal cancer (CRC and gastroesophageal cancer) have been developed and used to investigate if organoids can predict patient response to treatment [56] using a compound library of drugs already in clinical use or still on clinical trials. This study was carried out testing the sensitivity of organoid to drugs and comparing the outcome with the patient’s response. The results show that patient derived organoids recapitulate patient response in

clinical trials and therefore could be used for precision medicine programs. Another important advantage related to the organoids usage for drug testing is the capability to form organoids both from healthy and cancer tissue: this feature could be used to screen drugs that potentially affect tumoral cells while leave healthy cells unaffected. Most likely, this approach result in reduced toxicity in patients. Since most tumors have unstable genomes, tumor cells within a tumor contain different genes alterations. Even though it is believed that intratumoral heterogeneity contribute to cancer progression and resistance to therapy, it is still to be understood how tumor heterogeneity arises and play a role on the tumor progression. The heterogeneous genetic composition of a tumor is maintained in the derived organoids and remains over time in culture. Organoids can also be used to test if, with the repairing of a particular oncogene mutation, it could be restored the tumorigenic phenotype. However, it is not clear if the organoid approach can be translated also to non-epithelial tumors. But, although these limitations, organoids have emerged as physiologically relevant in vitro models for studying cancer [7].

1.5 Purpose of the work

In order to accomplish the project developed during these three years, three main goals needed to be addressed. The first one was to develop a device able to assess the diffusivity of free and nanoparticulate drugs. It is well known that when a drug is systemically or locally administered, it needs to reach the target pathological site crossing different barriers; one of them is the extracellular matrix. For the purpose of this project, it was important to create an easy device that could be used as preliminary tools to investigate the mobility of nanomedicines in the extravascular space. Biological barriers hampered the transport of nanotherapeutics to the disease site and this certainly prevents the good efficacy of these drugs. For this reason, we have tried to use strategies to allow nanoparticles have a greater mobility in crossing the extracellular matrix. For simplicity, in this work, the extracellular matrix has been realized and outlined only with type 1 collagen even if the resulting tool is general: versatility is its strong point. As first goal, attempts were made to create a simple device able to include an extracellular matrix model to test the diffusion of the beforehand nanoparticles. Attention has been paid to the different surface functionalization as a parameter, keeping the size of our nanotherapeutics constant to understand how surface properties influence their mobility and, therefore, understand in which direction act to improve their diffusion within tissues. For this reason, choosing the nanoparticles size of 200 nm as a basis, we have modified the surface with PEG at a different covering percentage and with HA at different molecular weight. It is known that PEG increases the half-life of nanotherapeutics, as happened for example with the liposomal covering of doxorubicin to which pegylation gave an increase from minutes to hours of the half circulating life [57] [58] as well as the

escape of the mononuclear phagocyte system by covering the particles with PEG. Therefore, in the first part of the project the effect of different PEG percentage on different nanoparticle surface have been dissected to see how much the pegylation affected the particle mobility. More precisely, the solidity of the procedure was verified using two different methods of diffusion study: one applicable only to the molecules (the fluorescence recovery after photobleaching) and one applicable both to molecules and nanoparticles (the mean square displacement (MSD) approach). Using the molecules as test for the two different procedures, the agreement between their outcomes elected the MSD as a strong and reliable method to assess the diffusion coefficient of nanomedicines. Using fluorescence recovery after photobleaching and mean square displacement for calculating the diffusion of molecules with different molecular weights (Dextran 4, 40, 250 kDa) values have been obtained according to each other. Once verified the solidity of the method, the MSD was used to calculate the diffusion of nanoparticles with different percentage of PEG on the surface. It was found that, for the same size, the greater superficial PEGylation resulted in greater particle mobility due to the lubricating effect of this polymer. Accordingly, we tried also with a different compound, the hyaluronic acid (HA), with two different aims: one is to understand if this naturally present compound in the human body as well as in the ECM of the brain and other tissues could be uses as a lubricant as well and, at the same time, using this lubricated nanotherapeutics to selectively target the CD44 receptor overexpressed by glioblastoma cells. Starting from liposomes of the same 200 nm size, we tested two different (MW) molecular weight HA. Surprisingly, we found that the diffusion was hampered as the HA molecular weight increased. It seems related to the more entanglement with the collagen matrix in which the NPs were tested for their diffusivity. The first and the second goal of this PhD project

were assessed as below: realizing an easy tool to study the diffusion and, studying the diffusion, discriminate between different surface decorations in order to find the more diffusive nanocarrier. It is common procedure, from some year to now, to try to use these models to prevent massive use of animals when it can be done without. For this reason, and to make the procedure even more general and solid, our NPs with different surface functionalization have also been tested in the mouse striatum, in brain slices try to keep them in similar alive fashion. Following the multiple particle tracking methods and analyzing the movement of these particles for their diffusion, we found there the same trend discovered within the collagen even if with different order of magnitude.

The first step in this process begins with the in vitro test of drugs and their delivery methods. Typically, these delivering tests are carry out in 2D cell cultures: most of cell-based assays use 2D monolayer cells cultures despite they have well known limitations [38]. They poorly mimic the in vivo condition: indeed, the absence of in vivo physiological processes don't allow them to accurately predict in vivo toxicity and other biological effects [39]; this lack, can severely compromise the reliability and significance of data obtained from 2D approaches [40]. 3D cell culture could surely offer better models for drug delivery toxicity tests than conventional 2D cultures. The reason of that assumption lies in their more realistic reproduction of physiological cell-cell contact geometry, mass transport, and tumor mass mechanical properties. The most common methods of culturing cells in 3D is allow cells to form spheroids: spherical cell clusters spontaneously formed [41]. They could be obtained using different techniques designed to promote the aggregation between the cells while avoiding the interaction cell-contact surface [42].

The third aim of this project is to use the same extracellular matrix as a' scaffold' to establish the growth of cells derived from human colorectal cancer tissues in order to have a reliable preclinical tool to test drugs and or nanodrugs. In order to do that, we establish a collaboration with the Galliera Hospital in Genova from which we got patients biopsies. We digested the tissue and we recreate, in *vitro*, the heterogeneity that the tumor has *in vivo*. We used this collagen matrix to place spheroids in a tissue familiar to them and we started using the tool to test drugs already in a clinical trial in order to assess the device. This has been done in order to use the tissue chamber chip and to test in real tumoral tissue different nanoparticles with different superficial decoration in order to effectively carry on and deliver the right cargo directly to the tumor. The tumoral spheroid was assessed for their heterogeneity using immunofluorescence and labeling for both colon cancer and stem cell markers.

Chapter 2

2. A tissue Chamber chip for assessing nanoparticle mobility in the extravascular space.

2.1 Background

Although a plethora of nanoparticle configurations have been proposed over the past 10 years, the uniform and deep penetration of systemically injected nanomedicines into the diseased tissue stays as a major biological barrier. Here, a 'Tissue Chamber' chip is designed and fabricated to study the extravascular transport of small molecules and nanoparticles. The chamber comprises a collagen slab, deposited within a PDMS mold, and an 800 μm channel for the injection of the working solution. Through fluorescent microscopy, the dynamics of molecules and nanoparticles was estimated within the gel, under different operating conditions. Diffusion coefficients were derived from the analysis of the particle mean square displacements (MSD). For validating the experimental apparatus and the protocol for data analysis, the diffusion *D* of FITC-Dextran molecules of 4, 40 and 250 kDa was first quantified. As expected, *D* reduces with the molecular weight of the dextran molecules. The MSD-derived diffusion coefficients were in good agreement with values derived via fluorescence recovery after photobleaching (FRAP), an alternative technique that solely applies to small molecules. Then, the transport of six nanoparticles with similar hydrodynamic diameters (~ 200 nm) and different surface chemistries was quantified. Surface PEGylation was confirmed to

favor the diffusion of nanoparticles within the collagen slab, whereas the surface decoration with hyaluronic acid (HA) chains reduced nanoparticle mobility in a way proportional to the HA molecular weight. To assess further the generality of the proposed approach, the diffusion of the six nanoparticles was also tested in freshly excised brain tissue slices. In these *ex vivo* experiments, the diffusion coefficients were 5-orders of magnitude smaller than for the Tissue Chamber chip. This was mostly ascribed to the lack of a cellular component in the chip. However, the trends documented for PEGylated and HA-coated nanoparticles in vitro were also confirmed ex vivo. This work demonstrates that the Tissue Chamber chip can be employed to effectively and efficiently test the extravascular transport of nanomedicines while minimizing the use of animals.

Here, a Tissue Chamber capable of studying the diffusivity of particles through an extravascular tissue-mimic in real-time is reported. Importantly, this research aimed to show as a proof-of-principle that the Tissue Chamber chip platform could quickly evaluate particle diffusivity and observe how particle properties could be optimized to facilitate diffusion through the tissue. The Tissue Chamber was realized by fabricating a collagen gel containing a cylindrical tube throughout the center. The transport properties of small-molecule fluorescent dyes (FITC-labelled dextran with varying molecular weights), 200 nm polystyrene beads or spherical PLGA nanoparticles coated with different amounts of poly (ethylene glycol) (PEG), and liposomes coated with different molecular weight hyaluronic acids (HA) were determined through fluorescent microscopy. Image analysis was then performed to evaluate the Mean Square Displacement (MSD) and subsequently the diffusivity of these different agents. Finally, ex vivo diffusion studies were performed in freshly excised brain tissue slices.

2.2 Experimental procedure

Materials

Collagen type I (4 mg/ml) from bovine origin and dextran with different molecular weights 4, 40, and 250 kDa were purchased from Sigma Aldrich (Sigma Aldrich, USA). Dulbecco's Phosphate Buffered Saline (DPBS) was acquired from Gibco Life technologies UK and Fluoresbrite™ carboxy nyo 0.20 μm microspheres were purchased from Polysciences, Inc. (Warrington PA). Poly(lactic-co-glycolic acid) PLGA (50:50, carboxy-terminated, MW 38,000-54,000 Da) was purchased from Sigma Aldrich (St. Louis, MO, USA); 1,2-dipalmitoyl-sn-glycero-3-phosphocholine (DPPC), DSPE-PEG(2000) Carboxylic Acid, DSPE-RhB (Liss Rhod PE), DSPE-EGG, 1,2-Dipalmitoyl-*sn-glycero*-3-phoshoethanolamine (DPPE) and cholesterol (Chol) were obtained from Avanti Polar Lipids (Alabaster, Alabama). Pure soybean phosphatidylcholine (Phospholipon 90G) (PC) was a kind gift from Phospholipid GmbH (Germany). Sodium hyaluronate was purchased from Lifecore Biomedical, LLC (MN,USA). O.C.T. mounting medium compound for cryotomy was purchased from VWR Chemicals. Permount Mounting Media was purchased from Fisher Scientific.

Synthesis of spherical polymeric nanoconstructs (SPNs)

Spherical Polymeric Nanoparticles (SPNs) tagged with different amounts of PEG were prepared by a slightly modified sonication-emulsion technique according to previously described procedures [59]. Two different configurations were prepared to obtain SPNs tagged with 80% or 20% of PEG on the outside surface. On both preparations, 20% of DSPE-RhB was included. Briefly, carboxyl-terminated PLGA and DPPC, in a 10:1 ratio, were dissolved in chloroform to obtain a homogeneous solution (oil phase). For the surface lipid monolayer with 80% PEG, two lipids were used (DSPE-PEG-COOH and DSPE-RhB) with a molar ratio of 5:1, dissolved in aqueous phase (4% ethanol). For the surface lipid monolayer with 20% PEG, three lipids were used (DSPE-PEG-COOH, DSPE-RhB and DSPE-EGG) with a molar ratio of 1:1:3, dissolved in aqueous phase (4% ethanol). The ratio between the oil phase and the aqueous phase was 1 to 5. Afterwards, the oil phase was added drop wisely to the aqueous phase under ultrasonication. The obtained emulsion was then placed under magnetic stirring to facilitate solvent evaporation. SPNs were centrifuged first for 5 minutes at 254 g to settle down any possible debris and then the supernatant was centrifuged 3 more times for 20 minutes at $1{,}8 \cdot 10^4$ g.

Preparation of liposomes

Liposomes were synthesized according to previously published procedures [60]. With minor modifications, Multilamellar Vesicles (MLVs) were made by a mixture of PC, Chol and DPPE in a molar ratio of 60:20:20 [61] [62]; [63]; [64]. In brief, lipids were dissolved in ethanol, dried under reduced pressure in a rotary evaporator (Buchi Rotary Evaporator Vacuum System Flavil, Switzerland) and afterwards were hydrated using a PBS solution at pH 7.4. MLVs also contained 0.5% Cy5 labeled DPPE [60]. At the end, MLVs were vortexed followed by 2 h of incubation in a shaker bath at 37 °C. Then, MLVs were extruded by the use of Lipex extrusion device (Northern lipids, Vancouver, Canada) at 65 °C and under 200-500 psi nitrogen pressure. Extrusion was accomplished in several steps using decreasing pore-size polycarbonate membranes (Whatman Inc., UK), performing numerous cycles per pore-size, in order to obtain unilamellar vescicles with a size ranging between 100 and 200 nm in diameter.

Surface modifications of liposomes

The liposome surface modification was made according to previous reported procedures [65]. In brief, high and low molecular weight hyaluronic acid (700 and 5kDa, respectively) were dissolved in 0.2 M MES buffer (pH 5.5) to reach a final concentration of 5 mg/ml or 40 mg/ml. Hyaluronic Acid (HA) was activated for 30 minutes with ethyl-dimethyl-aminopropyl-carbodiimide (EDC) (Sigma-Aldrich, USA) and sulfo-NHS (Proteochem) using a molar ratio of 1:1:6 between HA, EDC and sulfo-NHS. Afterwards, liposomes were added and pH was adjusted to 7.4. The solution was then incubated at

room temperature for 2 h and the free HA was removed by washing via centrifugation at 4 °C for 60 minutes at $1.3 \cdot 10^5$ g.

Size and stability characterization of nanoparticles

Dynamic light scattering (DLS, Malvern Zetasizer Nano S) was employed to characterize the size and zeta (ζ) potential of nanoparticles under hydrated conditions at pH 7.0. Nanoparticle stability was performed in water at 37 °C, following the size variation through DLS measurement. The same instrument was used to determine liposomes size and ζ potential for 5 days at 37 °C using HEPES 1M for the size and DI water for the ζ potential.

Tissue Chamber fabrication

The Tissue Chamber device was fabricated with polydimethylsiloxane (PDMS) using a pre-polymer solution of Syligard 182 mixed with the curing agent in a 10:1 ratio w/w. This solution was poured in a petri dish to create a 3.5 mm thick PDMS sheet. The petri dish with PDMS was degassed in a vacuum chamber and cured in the oven at 60 °C overnight. After 15 minutes at room temperature the petri dish was cooled to -20 °C for 1 h before removing the sheet from the base. The PDMS sheets were cut into 15 × 15 × 3.5 mm^3 parallelepipeds, and a 5 × 5 × 3.5 mm^3 empty space for the Tissue Chamber was cut into the center. The PDMS Tissue Chamber was irreversibly bonded to a glass microscope slide (VWR) using oxygen plasma. At the end of the process, a 21 G (0.8 mm diameter) needle (Sterican B. Braun) was used to generate a channel in the Tissue

Chamber from side to side. At the very end, chips were sterilized by autoclave and dried in an incubator overnight. **Figure 2.1** illustrates the Tissue Chamber fabrication and final geometry.

Collagen type I gel preparation

Collagen type I pH and ionic strength were adjusted by addition of the buffer solution (pH 7.4) to achieve a final pH between 7 and 7.4, with a final concentration of 1.5 mg/ml. 150 μl of collagen type I solution was injected inside the Tissue Chamber and polymerization occurred at 37 °C for 1 h. Next, gels were covered with 50 μl of DPBS to keep them in a hydrated state. After one hour, the needle was removed and the channel was confirmed by optical microscope images (**Figure 2.1**).

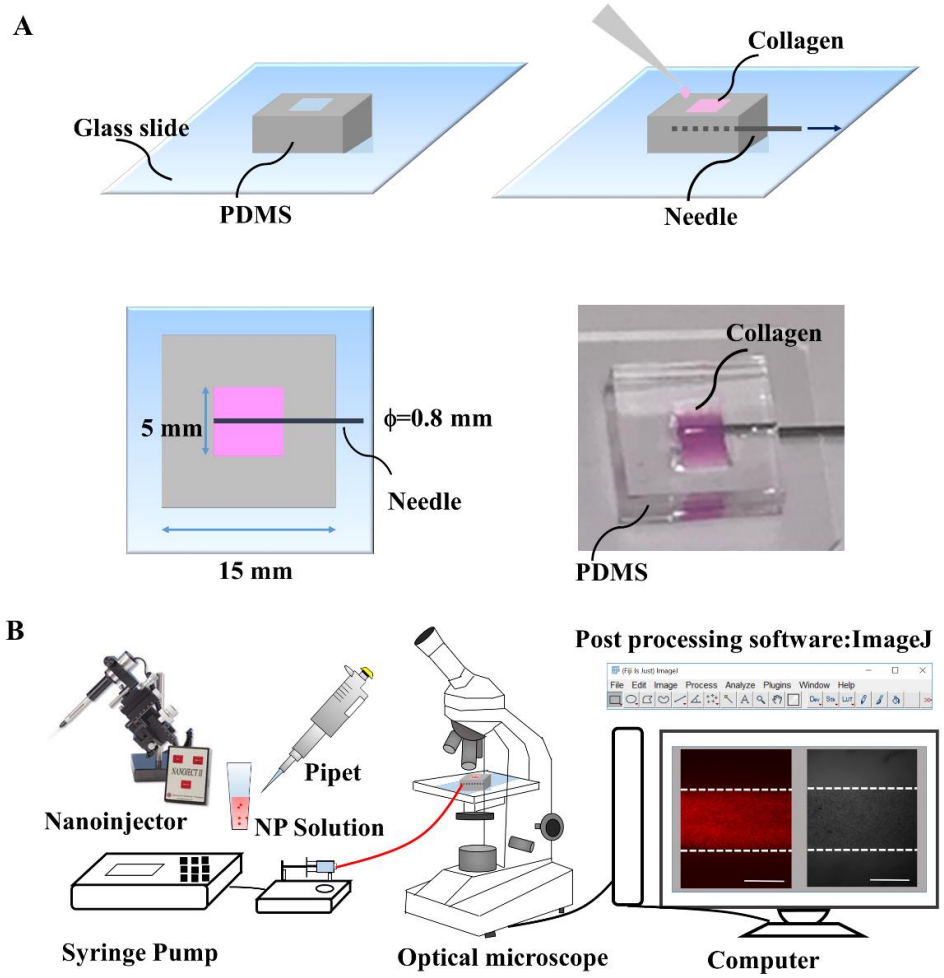

Figure 2.1 *Tissue Chamber microfluidic chip: A. 3D schematic representation of the Tissue Chamber PDMS chip with a description of channel fabrication process, an overhead view of the Tissue Chamber showing the dimensions, and a photographic image of the Tissue Chamber bonded on a glass slide and filled with collagen type I. The photograph shows the needle inserted across the chamber, which is used to create the channel for injecting tracers. B. Schematic of the entire experimental setup with representative optical microscopy images of 200 nm beads injected inside the channel: brightfiled (right) and fluorescent (left) images of a channel portion. Scale bars are 500 μm.*

Diffusion assays

Samples were placed under an inverted optical microscope (Leica DMI 6000 B) equipped with a DFC360 FX digital fluorescence camera. Different molecules and particles were injected to study the diffusion through the collagen hydrogel: Dextran 4, 40 and 250 kDa, 200 nm Fluoresbrite® carboxylate microspheres, SPNs and liposomes with different PEG and HA amounts. Fluoresbrite® carboxylate microspheres (from now on called NP 200) are commercially available monodispersed fluorescent polystyrene microspheres. These microspheres were provided as 2.5% aqueous suspensions and injected in the Tissue Chamber at 0.05% (w/v), SPNs 20% PEG and SPNs 80% PEG were injected at the same ratio (0.05% w/v). Solutions of Dextran 4, 40 and 250 kDa were injected at 0.5 mg/ml and the 3 different kinds of liposomes were injected at stock concentrations (lipid 40 mg/ml). Images were collected every 30 seconds for 4.5 minutes for the Dextran 4, 40 and 250 kDa (5 μl); every minute for 10 minutes in the case of NP 200; every 4 seconds for 44 seconds for all SPNs and liposomes (5 μl).

Mean square displacement (MSD)

By tracking the colored wave-front inside the Tissue Chamber collagen over time, the overall diffusion coefficient D in one dimension (1D) was determined as

$$D = \frac{MSD}{2T} \tag{2.1}$$

where T is the time interval and the MSD were calculated from:

$$MSD_{1D} = < \Delta x(j\Delta t)^2 > \tag{2.2}$$

While the more general formula, for the 3D diffusion is:

$$MSD_{3D} = < \Delta x(j\Delta t)^2 + \Delta y(j\Delta t)^2 + \Delta z(j\Delta t)^2 > \quad (2.3)$$

With the j index running on the total number of Δt in T and x represents the height of colored channel at time t [66]. The area of the channel perfused by the working solution is rectangular with the long edge aligned with the 800 μm injection channel and the short edge corresponding to the distance traveled by the working solution into the collagen matrix. This distance is calculated by post processing the fluorescence pics via Fiji. Notice that this distance is also the distance traveled by the molecules, or nanoparticles, over time and corresponds to the displacement in the MSD analyses. Following Xavier (2010) [67] , the MSD is calculated on all the experimental points while the diffusion coefficient is obtained by linearly interpolating the points falling in the first quartile of the MSD curves. Using the conventional formula in eq. (2.1), the diffusion coefficients were determined as half of the slope of the curve fitting the MSD points in the first quartile.

Fluorescence recovery after photobleaching (FRAP)

In this analysis, experiments were conducted using a Nikon A1R confocal laser scanning microscope with a Plan Apo DIC N2 20×/ 0.75 objective. A 488 nm Argon ions laser line was used to excite the samples and a bandpass 500-550 filter was placed before the photomultiplier tube. The collagen solution was placed in μ-Dish Micro-Insert 4 well (Ibidi, Germany) and 10 μl of neutralized collagen type I was polymerized at 37 °C for 1 h. Each tissue construct was injected with 23 nl using a nanoinjector (Drummond "Nanoject II" automatic nanoliter injector), following manufacturer's instructions. Injection velocity was 23 nl/s. The Nanoject II required pulled micropipets with a

capillary outer diameter of 1140 μm and inner diameter of 530 μm. Experiments were performed at equilibrium, generally 12-48 hours post injection depending on the MW of the molecule. Using a circular region of interest (ROI) with a radius of 92.5 μm, gels were first photobleached with a laser for 20 minutes and then the recovery of fluorescence was observed in the following 20 minutes. The recovery of fluorescence in the bleached ROIs gave the diffusion coefficient. The software provides the curve associated with bleaching and recovery as well as the parameter τ_D, which is related to the diffusion coefficient through the following formula:

$$\tau_D = \frac{\omega^2}{4D} \tag{2.4}$$

*w*here ω is the radius of the ROI and D is the diffusion coefficient [3].

Quantification of the diffusion coefficient via error minimization algorithm (EMA).

This technique is useful when FRAP and MSD cannot be applied. It is rather general and robust as it takes as an input the raw data from the diffusion assays (**Figure 2.6**). An efficient algorithm for fitting a vector of parameters on a given dataset is developed [68]. The parameters are interpreted as control variables in an optimization problem that minimizes a functional representing the difference between the experimental observations and the model predictions. The collagen gel in the Tissue Chamber chip is described as a rectangular domain **Ω** in which, at the initial time, a concentration $c\ (x, y,0) = c_{inj}(x, y)$ of molecules is prescribed. The temporal evolution of the concentration $c = c(x,y,t)$ in the time interval $[0, T]$ is described by:

$$\begin{cases} \frac{\partial c}{\partial t} - D\Delta c = 0 & \text{in } \Omega, t > 0, \\ D\nabla c \cdot \boldsymbol{n} = 0 & \text{on } \partial\Omega \times (0,T), \\ c = c_{inj} & \text{in } \Omega, t = 0, \end{cases} \tag{2.5}$$

where $\Delta u = \partial_{xx}u + \partial_{yy}u$ is the Laplace operator and $c_{inj} = c_{inj}(x,y)$ is an assigned function obtained processing the fluorescence images at time $t = 0$ using the algorithm summarized in steps 1, 2, 3, 4 described in what follows. The system can be readily solved numerically if *D* is known (direct problem). For the inverse problem, *D* is not known a priori. In this case, the solution is obtained by minimizing the following functional *J*:

$$\min J(D) = \frac{1}{2}||c(T) - \bar{c}(T)||^2_{L^2(\Omega)} + \frac{\lambda}{2}|D|^2, \tag{2.6}$$

subject to the eq. (2.6). The first term in *J* gives the difference between the experimentally observed concentration field $\bar{c}$ at *T* and the concentration field c , which is computed at time T using eq. (2.6) under a specific assumption for *D*. The second term $\frac{\lambda}{2}|D|^2$ is a regularization operator. For the Lagrangian principle, the optimal diffusion parameter is the solution of the unconstrained minimization problem $\min \mathcal{L}(c, D, p)$ where $\mathcal{L}$ is the Lagrangian functional, defined as follows

$$\mathcal{L}(c, D, p) = J(c, D) - \int_0^T \int_\Omega \frac{\partial c}{\partial t} p - \int_0^T \int_\Omega D\nabla c \cdot \nabla p \tag{2.7}$$

where *p* is the so-called Lagrange multiplier. For the space discretization, an admissible triangulation of the domain **Ω** is introduced and the linear finite element method is applied (**Figure 2.6**). For time discretization, the backward Euler scheme is chosen. To evaluate the functional *J*, the finite element approximation of the state equations must be compared with the observed concentration field $\bar{c}$. To this end, the pixel map of $\bar{c}$ is converted into

a finite element function. This is achieved by means of image analysis tools as per the following protocol: 1. Conversion of the RGB picture for $\bar{c}$ into a gray scale image; 2. generation of a mesh with triangular elements having the same dimensions as pixel number of the image; 3. definition of a finite element variable that accounts for the grey level for each pixel; 4. projection of the previous gray scale map on a coarse mesh of triangular elements used for the solution of the finite element method applied to eq. (2.6).The minimization of the Lagrangian functional is achieved by means of a Non Linear Conjugate Gradient iterative method, which, given a starting value for D, solves eq. (2.6), then computes the functional *J*, solves for the adjoint equation to estimate *p*, and evaluates the derivative of $\mathcal{L}$ with respect to D. If this is sufficiently close to zero then the correct value for D is returned. If this is not close to zero, then it updates the diffusion coefficient estimation and it runs again the full analysis starting a new iteration

Ex vivo experiments

Wild-type C57BL/6 mice aged 2-6 months were sacrificed to obtain 2.0 mm brain tissue slices via a Zivic Mouse brain slicer. The striatum of these tissues was injected with 69 nl of a solution containing approximately 1,000 nanoparticles for each experiment using the nanoinjector with a velocity of 23 nl/s. Injected slices were placed in a custom-made, three-dimensional (3D) particle tracking system consisting of a wide-field inverted microscope (Nikon Ti) with an oil-immersion objective (Nikon Plan Apo VC 100×/1.4 oil DIC N2), a piezoelectric stage (Mad City Lab) and a single EMCCD camera (DU897DCS-BV Andor Technology) [69];[70]. Sequential images of multiple

nanoparticles were recorded at 10 frames per second (fps) in time slots of 40 s [70]. At the end, the 3D particle trajectories and the corresponding MSD were calculated by post processing the movies with Fiji [71] and a custom MATLAB script.

2.3 Experimental results and discussion

The Tissue Chamber apparatus for the diffusion experiments

The Tissue Chamber chip forms a 5 × 5 × 3.5 mm^3 parallelepiped. **Figure 2.1 A** shows a schematic representation of the fabrication process to realize the Tissue Chamber chip. The pink fluid is related to a collagen solution that is cast around a 21G needle (black line), which is used to realize the channel for dispersing small molecules and nanoparticles within the chip itself. The needle outer diameter is equal to 800 μm (ϕ = 0.8 mm). This size was chosen in order to ensure the mechanical stability of the channel, and thus prevent its collapse and closure. Furthermore, it should be highlighted that the overall width of the Tissue Chamber (5 mm) is significantly larger than the channel diameter (0.8 mm). This size ratio ensures that any boundary effects in the transport process can be neglected, while still realizing a working region that could be observed with a 4× objective. **Figure 2.1 B** shows the different steps in the analysis, which includes the chip fabrication; the injection of the test solution (e.g. dextran-dye or particles) via a pipette NanoInjector or syringe pump; the microscopy acquisition, image post-processing and mathematical analysis. Specifically, in order to perform the diffusion measurements, the Tissue Chamber is placed on the stage of an inverted optical microscope, and images were acquired following the administration of fluorescent dextran or particles. Images are post-processed using Fiji (https://imagej.nih.gov/).

Analysis of the diffusion of small molecules within the Tissue Chamber chip

In order to test the chip and the whole measurement apparatus, dextran molecules of different molecular weights were used. Specifically, 5 μl of an aqueous solution containing 4, 40 or 250 kDa FITC-dextran molecules were injected into the Tissue Chamber. The progressive spreading of the green fluorescent solution within the gel is recorded over time. The three top rows of **Figures 2.2A-C** present the diffusing front of the dextran solutions at different time points, namely 0, 90 and 240 sec. At each time point, the size of the colored area is estimated by post-processing the fluorescent images via the Fiji software. Note that the size of the channel is about 800 μm, which corresponds to the outer diameter of the needle used for realizing the channel itself within the collagen matrix. The lowest row in **Figures 2.2A-C** shows the variation over time of the averaged MSD, calculated from the experimental data using eq. (2.2) in the Methods section. Each point on these plots corresponds to the MSD at that time *t*, averaged over multiple experiments ($n \geq 5$). The slope of the MSD (t) curves provides, through eq. (2.1) the actual diffusion coefficient. **Figure 2.2 D** summarizes the experimental results providing the diffusion coefficient of the three tested molecules (4, 40 and 250 FITC-dextran) as derived from the MSD measurements in the Tissue Chamber chip (blue bars). As expected, the diffusion coefficient reduces as the molecular weight of dextran increases. For the 4 kDa dextran, a coefficient of diffusion $D = 44.20 \pm 6.65$ $\mu m^2/s$ is derived. This number reduces by about 49% ($D = 22.4 \pm 16.8$ $\mu m^2/s$) for 40 kDa dextran, and by about 78% ($D = 9.9 \pm 3.71$ $\mu m^2/s$) for 250 kDa dextran.

The Einstein-Stoke relation was used to estimate the diffusion coefficients of the dextran molecules in pure water:

$$D_w = \frac{k_B T}{(6\pi\mu R_H)}$$

(2.8)

from which it results that $D_w < 270$ μm^2/s for 4 kDa dextran, < 40 μm^2/s for 40 kDa dextran, and < 20 μm^2/s for 250 kDa dextran. Indeed, as expected, the diffusion coefficient in water is significantly higher than in the collagen matrix for all dextran molecular weights. However, interestingly, it is the dextran with the smaller molecular weight (4 kDa) that is subjected to the largest reduction (6-fold) in diffusion from <270 to <45 μm^2/s. In eq. (2.8), k_BT is the Boltzmann energy at room temperature ($4.11 \cdot 10^{-21}$ J), μ is the dynamic viscosity of water (10^{-3} Pa·s), and R_H is the hydrodynamic radius of the molecule ($R_H < 0.8$ nm for 4 kDa dextran, < 5 nm for 40 kDa dextran, and < 11.5 nm for 250 kDa dextran) [72]. To validate the experimental set-up, the diffusion of dextran molecules in collagen was also assessed via Fluorescence Recovery After Photobleaching (FRAP) returning values in good agreement with those quantified within the Tissue Chamber chip. Specifically, the diffusion coefficients estimated via FRAP were equal to $D_{FRAP} = 37.30 \pm 5.06$ μm^2/s for 4 kDa dextran, 15.20 ± 3.14 μm^2/s for 40 kDa dextran, and 10.10 ± 2.06 μm^2/s for 250 kDa dextran. Finally, the diffusion coefficient was also estimated via the EMA approach and compared with the MSD and FRAP results. The EMA was applied using a regularization parameter $\lambda = 10^{-2}$. The diffusion coefficient was computed as the average of the diffusion coefficients resulting from the analysis of different time intervals. In particular, $D_{EMA} = 81.15 \pm 63.09$ μm^2/s for 4 kDa Dextran, 49.15 ± 19.73 μm^2/s for 40 kDa Dextran and 13.54 ± 5.38 μm^2/s for 250 kDa Dextran. Interestingly, the higher is the Dextran molecular weight, the smaller is the difference between the results obtained using the EMA and MSD.

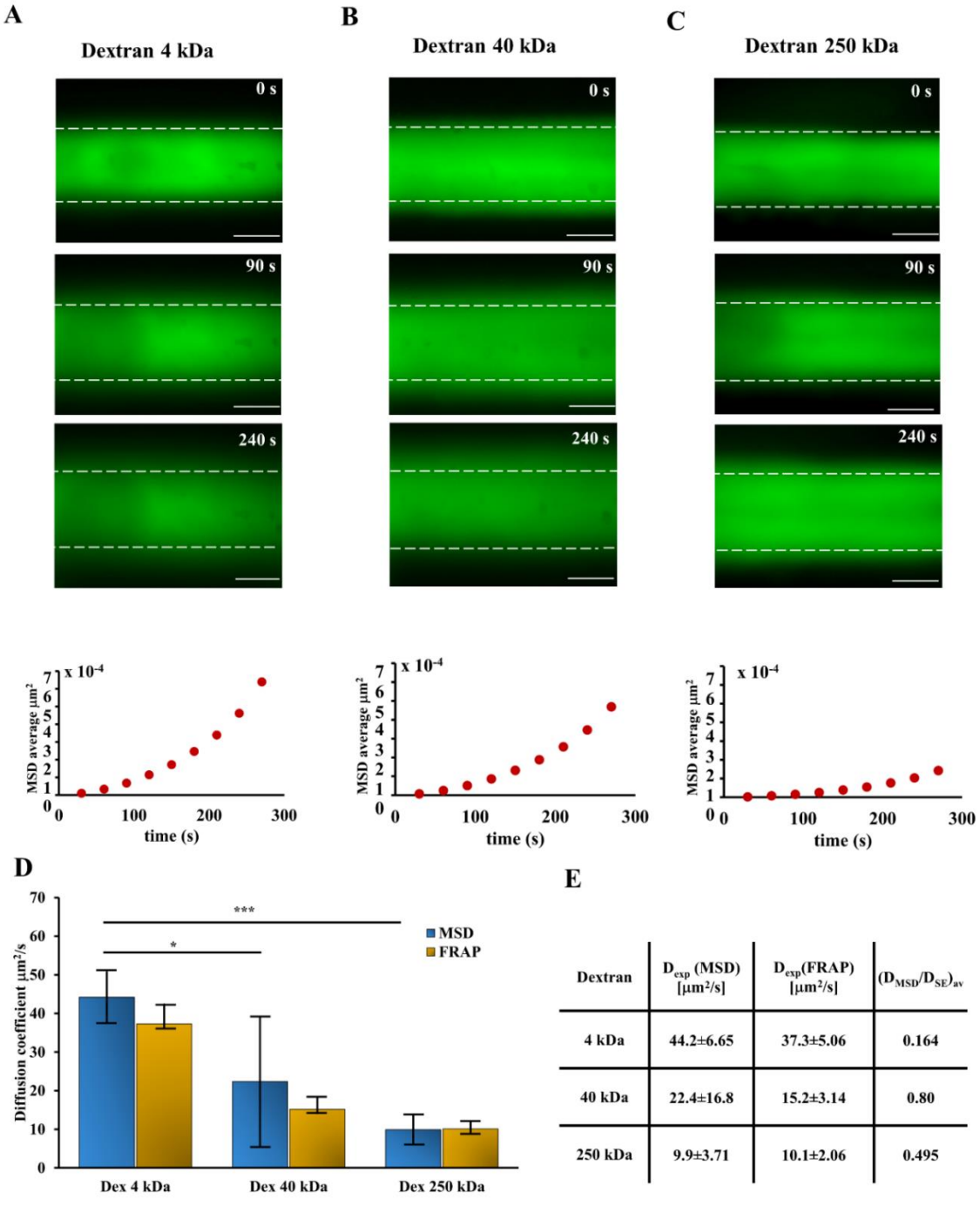

Dextran	D_{exp} (MSD) [µm²/s]	D_{exp}(FRAP) [µm²/s]	$(D_{MSD}/D_{SE})_{av}$
4 kDa	44.2±6.65	37.3±5.06	0.164
40 kDa	22.4±16.8	15.2±3.14	0.80
250 kDa	9.9±3.71	10.1±2.06	0.495

Figure 2.2 Optical fluorescent microscopy images and quantification of different molecular weight Dextran diffusion. *A. Fluorescent images of the channel in the Tissue Chamber filled up with Dextran 4 kDa acquired at different time point (0 s, 90 s, 240 s) and averaged values of the Mean Square Displacement (MSD); B. Fluorescent images of the channel in the Tissue Chamber filled up with Dextran 40 kDa acquired at different time point (0 s, 90 s, 240 s) and averaged values of the MSD; C. Fluorescent images of*

*the channel in the Tissue Chamber filled up with Dextran 250 kDa acquired at different time point (0 s, 90 s, 240 s) and averaged values of the MSD. Scale bars are 500 micron.**;** D. Bar chart of molecular diffusion coefficients obtained for molecules using two different analysis (MSD and Fluorescent Recovery After Photobleaching, FRAP); E.Summarized table of MSD and FRAP derived molecular diffusion coefficients for same dye as well as their experimental and theoretical diffusion ratio. Number of repetitions n>5 for MSD and n=4 for FRAP. * Symbol denotes statistically significant difference p<0.05, *** p< 0.001.*

Particle characterization

In this section, the diffusion of three different nanoparticles within the collagen matrix of the Tissue Chamber chip was studied systematically. In **Figure 2.3**, schematic representations (first row); scanning electron microscopy images (second row); and the temporal variation of size and surface ζ potential (third row) are presented for the three different nanoparticles: NP 200 – commercially available 200 nm polystyrene nanoparticles; SPN – spherical polymeric nanoparticles with all hydrodynamic diameter of approximately 200 nm; and HA-Lip – liposomes coated with a hyaluronic acid layer returning a hydrodynamic diameter around 200 nm.

The NP 200 nanoparticles have a carboxylated surface, a hydrodynamic diameter of 187.96 ± 2.42 nm and a ζ potential of -42.5 ± 2.12 mV. The stability of these particles was clearly demonstrated by the DLS data documenting a fairly constant hydrodynamic diameter over 5 days of observation (**Figure 2.3A**, third row). The ζ potential consistently stayed between -40 and -50 mV contributing to the electrostatic repulsion and therefore the colloidal stability of the NP 200. The electron microscopy images of **Figure 2.3A**

(second row) confirm the uniform spherical shape of these particles. The spherical polymeric nanoparticles (SPNs) were synthesized via an emulsion technique and possess a poly(lactic-co-glycolic acid) (PLGA) core stabilized by a lipid monolayer, with polyethylene glycol (PEG) chains [59] ;[73]. **Figure 2.3 B** (first row) shows a schematic representation of SPNs documenting the polymeric/lipid structure. Chains of lipid-RhB are included in the surface monolayer thus introducing fluorescent reporting molecules in the nanoparticle structure. Two different configurations of SPNs are realized depending on the initial PEG content. For 20% SPN, the initial concentration of lipid-PEG is 20% of the total lipid mass while, for 80% SPN, the initial concentration of lipid-PEG is 80% of the total lipid mass. In both cases, the electron microscopy analysis confirms the spherical shape and monodisperse size distribution of the nanoparticles (**Figure 2.3 B**, second row). At time zero, the DLS returns a hydrodynamic size of 186 ± 13 nm and a ζ potential of -45.9 ± 0.79 mV for the 20% SPNs. The 80% SPNs are slightly smaller with a hydrodynamic size of 170 ± 3 nm and a ζ potential of –39.1 ± 0.87 mV. Indeed, the higher percent of lipid-PEG on the SPN surface fosters stabilization, thus reducing the overall hydrodynamic diameter (**Figure 2.3 C**, third row). A similar behavior is observed of the HA-Lip particles. Notice that particle stabilization and size reduction have been well documented in the literature also by other authors (see for instance [74];[75]). The spherical polymeric nanoconstructs are stable over the period of 5 days with an overall variation in hydrodynamic size limited to 10% for both 20% and 80% SPNs (**Figure 2.3 C**, third row).

Finally, the third type of nanoparticles schematically presented in the first row of **Figure 2.3 C** are the liposomes with an aqueous core and a lipid bilayer, which is externally coated at different degrees with hyaluronic acid (HA) [60]. Three different configurations

of this HA-Lip are considered: liposomes not coated with any HA layer (uHA-Lip), liposomes coated with a 5kDa HA layer (5HA-Lip), and liposomes coated with a 700 kDa HA layer (700HA-Lip). For the uHA-Lip, the initial hydrodynamic diameter was 146.1± 4.271 nm. This decreases to 138.5 ± 4.845 and 132.4 ± 6.493 nm for the 5HA-Lip and 700Ha-Lip, respectively. The ζ potential is stable at -37 ± 4 mV for all three configurations. SEM and TEM images confirm the DLS data. Specifically, the electron microscopy images in **Figure 2.3 C** (second row) are for the 5HA-Lip (SEM) and for uHA-Lip (TEM). Furthermore, these nanoparticles present good colloidal stability over a 5-days period **Figure 2.3 C** (third row).

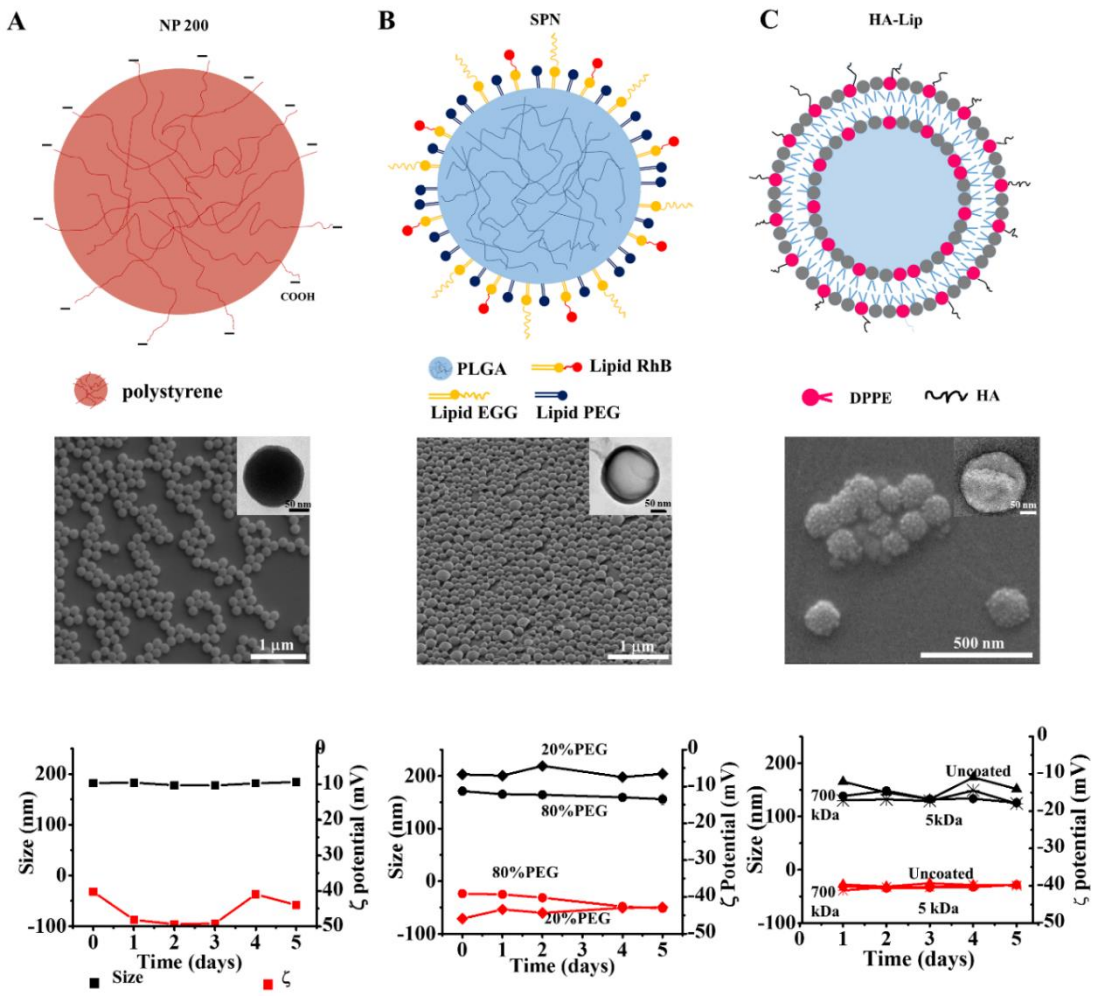

Figure 2.3 *Schematic representations, electron microscopy images, dynamic light scattering (DLS) hydrodynamic size and ζ-potential measurements for A. commercially available polystyrene carboxylate beads, B. spherical PEGylated PLGA nanoparticles, and C. liposomes coated with varying molecular weight hyaluronic acid. DLS and ζ-potential measurements were made over 5 days in water.*

Analysis of the diffusion of nanoparticles within the Tissue Chamber chip

After confirming the size and stability of the nanoparticles, diffusion experiments were conducted in the Tissue Chamber chip. Specifically, a 5 μl solution with SPNs or HA-Lip was introduced into the chip and the progressive diffusion within the collagen matrix was recorded over time. The bar charts in **Figure 2.4A** provides the diffusion coefficients in the collagen matrix for NP 200, the two SPN configurations, and the three HA-Lip configurations. Representative fluorescence image of 5HA-lip in the chip and their relative MSD curve in collagen are given in **Figure 2.4B**. It is shown that the diffusion coefficient increases from 1.75 ± 0.65 $\mu m^2/s$ for the NP 200, un-PEGylated nanoparticles, to 3.38 ± 1.89 $\mu m^2/s$ for the 20% SPNs and 4.89 ± 0.25 $\mu m^2/s$ for the 80% SPNs, which are characterized by the highest surface density of PEG. For the liposomes, the presence of HA over the surface reduces the diffusion coefficient from 5.01 ± 1.96 $\mu m^2/s$ for the uHA-Lip; to 3.83 ± 1.80 $\mu m^2/s$ for the 5HA-Lip and 2.21 ± 1.30 $\mu m^2/s$ for the 700HA-Lip. The theoretical diffusion coefficient through the equation of Einstein-Stokes was also calculated. The diffusion coefficients for the NP 200, 20% SPNs 20% PEG and SPNs 80% PEG using the EMA approach were also computed. In particular, $D_{EMA} = 1.75 \pm 0.65$ $\mu m^2/s$ for the NP 200, 21.40 ± 7.41 $\mu m^2/s$ for the SPNs 20% PEG and 6.68 ± 2.56 $\mu m^2/s$

for the SPNs 80% PEG. While the D_{EMA} values for NP 200 and 80% SPNs are in good agreement with the MSD-derived diffusion coefficients, EMA fails in predicting accurately the diffusion for the SPNs 20% PEG.

These results emphasize that an increase in PEGylation can more efficiently lubricate the particle-tissue interface and favor the diffusion and tissue penetration [76]. For the second group of nanoparticles studied, i.e. liposomes, the diffusion coefficient within the type I collagen gel calculated with the MSD shows that the uHA-Lip diffuse more than the HA coated liposomes, ostensibly due to the interaction of collagen with hyaluronic acid [77]. Moreover, the 5HA-Lip may diffuse more than 700HA-Lip for their greater lubricating effect [78].

A

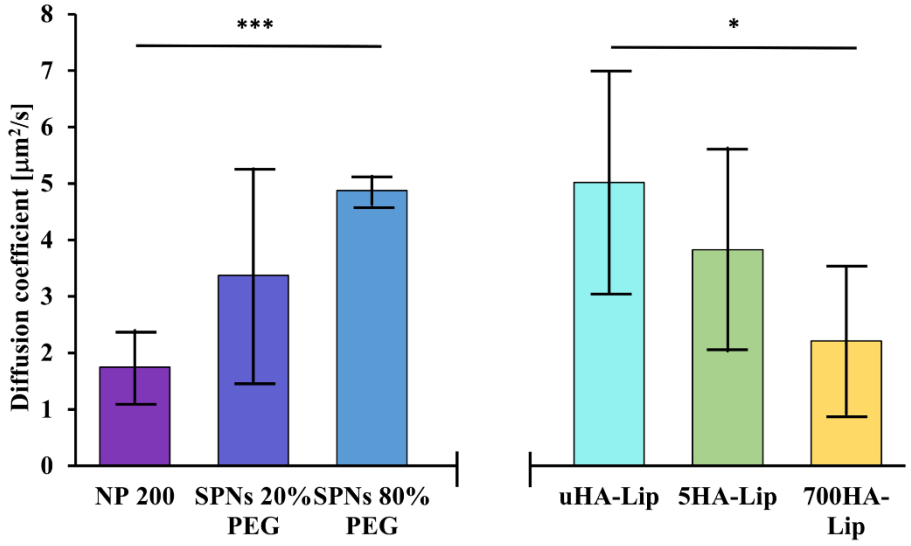

B

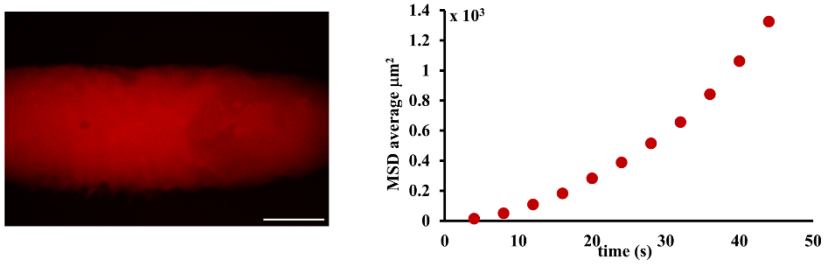

C

	Diameter (nm)	D_{MSD} [µm²/s]	D_{SE} [µm²/s]	$(D_{MSD}/D_{SE})_{av}$
NP 200	187.96±2.42	1.75±0.645	2.325	0.753
SPNs 20%PEG	186.2±13	3.38±1.89	2.347	1.440
SPNs 80%PEG	170.4±2.5	4.89±0.25	2.564	1.907
uHA-Lip	146.1 ±4.271	5.01±1.96	2.986	1.678
5HA-Lip	138.5 ±4.845	3.83±1.8	3.127	1.225
700HA-Lip	132.4 ±6.493	2.21±1.30	3.199	0.691

Figure 2.4 *A. Quantification of nanoparticles molecular diffusion coefficient in collagen gel was determined for nanoparticles using the MSD; B. Representative fluorescent images of 5HA-Lip injected inside the Tissue Chamber and the corresponding the MSD plot. Scale bar represents 500 µm; C. A table summarizing the nanoparticles diameters, and the MSD and Stokes-Einstein-derived molecular diffusion coefficients for the particles. N ≥ 4. * Denotes statistically significant difference p < 0.05, *** p<0.001.*

Analysis of the diffusion of nanoparticles within brain tissue slices

The diffusion of nanoparticles was also assessed in 2 mm thick, freshly excised brain slices from C57BL/6 wild-type mice. To avoid tissue death, brain slices were kept on ice and hydrated with cold PBS. A 69 nl of a solution containing the different types of nanoparticles was introduced in the striatum of the brain slices (**Figure 2.5A-C**). The Nanoinjector was placed at 1.5 mm from the top of the slice and the desired volume was introduced at 0.5 mm from the bottom of the slice [70]. The dynamics of the nanoparticles was monitored over time using an inverted microscope specifically modified for single particle tracking, using an oil immersion 100× objective. Representative images are provided in **Figure 2.5 C**. The resulting movies were post-processed through the Fiji trackmate tool [79] and analyzed with a custom Matlab script, which was specially developed to extrapolate the MSD [69];[67]. This custom MATLAB (version R2015a) script, was used to estimate the MSD and the diffusion coefficient of the different molecules and nanoparticles in ex vivo brain tissue.

From this analysis, 3D (x,y,z) trajectories of the individual particles over time can be extracted, as shown in **Figure 2.5 D**. Finally, the MSD of the nanoparticles can be computed and, consequently, the diffusion coefficient is derived as described in the previous paragraphs. The diffusion coefficient for the six different particles are provided by the bar chart in **Figure 2.5 E**. Notably, the trends are similar to the one derived for the same particle in vitro within the collagen matrix of the Tissue Chamber chip. In other words, the diffusion coefficient increase moving from un-PEGylated nanoparticles (NP 200) to PEGylated SPNs, and reduces with the presence of HA on liposomes. Specifically, the diffusion was $2.68 \pm 1.33 \cdot 10^{-5}$ $\mu m^2/s$ for the NP 200; $4.84 \pm 2.41 \cdot 10^{-5}$

$\mu m^2/s$ for the 20% SPNs; $5.36 \pm 2.49 \cdot 10^{-5}$ $\mu m^2/s$ for the 80% SPNs; $6.32 \pm 2.81 \cdot 10^{-5}$ $\mu m^2/s$ for the uHA-Lip; $3.50 \pm 1.91 \cdot 10^{-5}$ $\mu m^2/s$ for the 5HA-Lip; and $2.48 \pm 1.35 \cdot 10^{-5}$ $\mu m^2/s$ for the 700HA-Lip.

Comparing these results with the one obtained in the Tissue Chamber chip, a decrease in the diffusion coefficient of five orders of magnitude was noticed. This is indeed expected given that the Tissue Chamber chip does not include cells in its current configuration. But even if these differences in values, the observed trend of the diffusion coefficient depending on the pegylation and different MW HA coating is the same as in the Tissue Chamber chip. These results strengthen the solidity and the repeatability of the approach adopted for the study of diffusion coefficients of nanomedicines in various areas of the body, appropriately mimed using different substrates. Surely a versatile device like the Tissue Chamber could be further use in the future adding complexity to the collagen-based model to better approximate different biological districts.

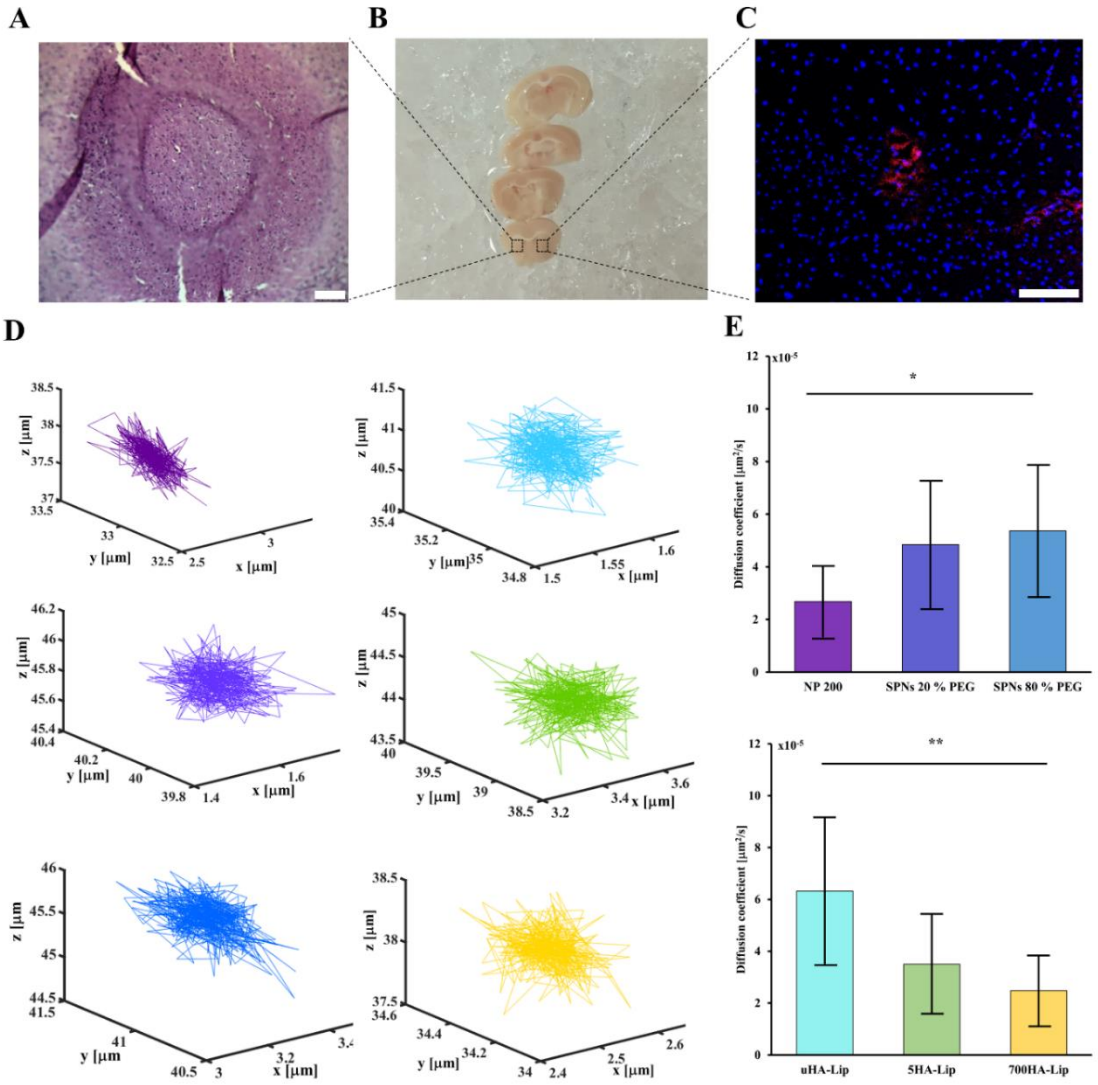

Figure 2.5 *Ex-vivo single tracking and quantification of nanoparticles molecular diffusion coefficient. A. Representative image of a 12 µm mouse brain slice stained with H&E with recognizable sign of the injection needle. Scale bar represents100 µm. B. Representative image of different brain sections. Squares highlight the striatum. C. Confocal fluorescent microscopy image of a brain slice shows the NPs as red spots and the nuclei stained in DAPI. Scale bar represents 100 µm. D. 3D trajectories of the particles diffusing through ex vivo brain slices. E. Diffusion coefficients obtained for nanoparticles in the ex vivo brain tissue derived using MSD analysis. * Denotes a statistically significant difference $p < 0.05$, ** $p < 0.01$.*

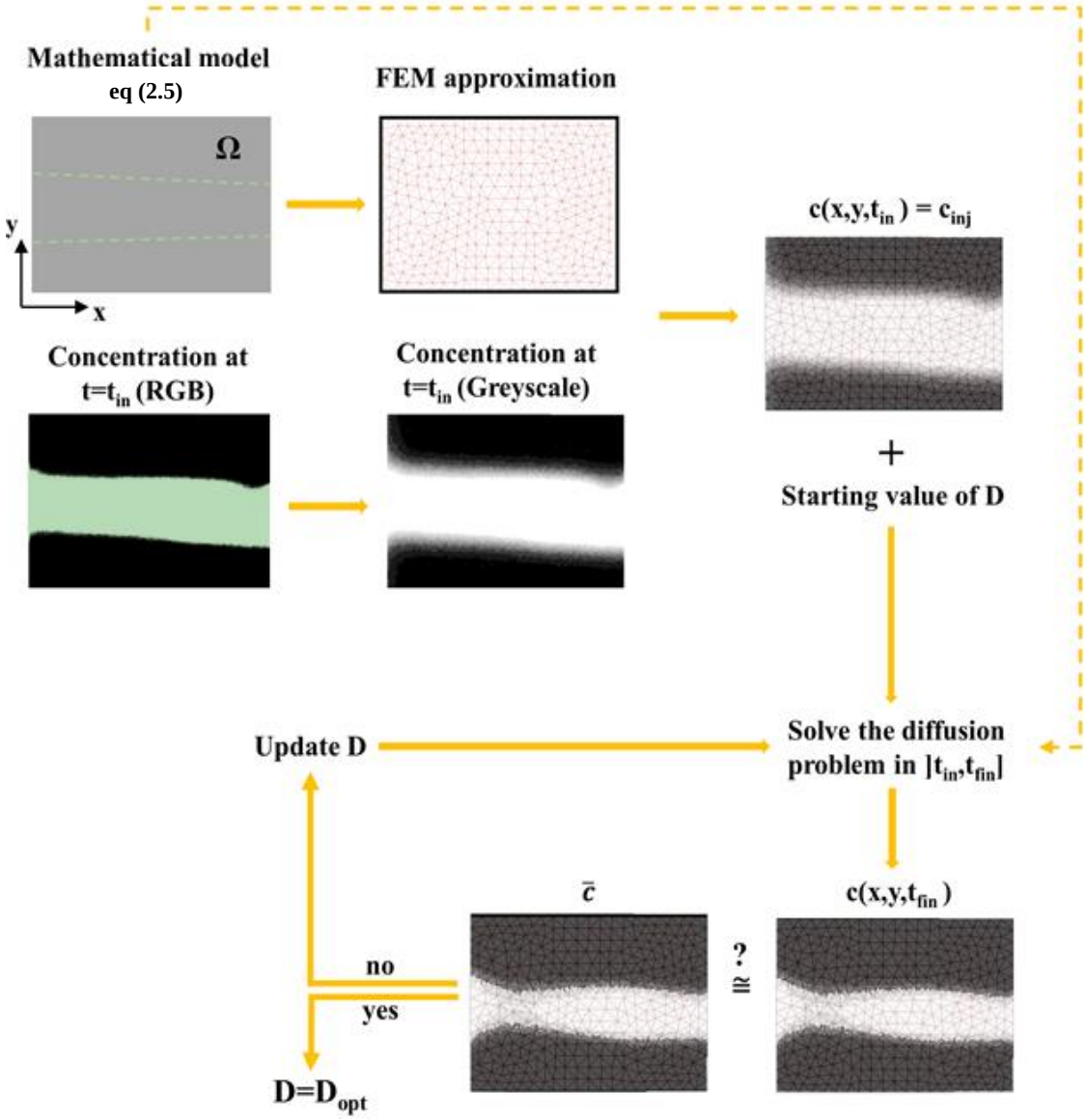

Figure 2.6 *Quantification of the diffusion coefficient via an error minimization algorithm. Post-processing of the experimental data with conversion of the fluorescent microscopy images into greyscale maps and error minimization procedure implemented in the computational algorithm.*

Figure 2.6 describes the EMA (Error Minimization Algorithm) presented in section Quantification of the diffusion coefficient via error minimization algorithm (EMA). More precisely, the schematic summarizes how the diffusion coefficient D is computed solving

the optimization problem (2.6). The collagen Tissue Chamber chip is represented in the numerical framework by a rectangular domain Ω (top).

Firstly, the image of the experimental concentration at the initial time t_{in} is converted into a gray scale image and it is projected on a triangular mesh of Omega. Then, the resulting Finite Element function is used as initial concentration c_{inj} in (2.5). Problem (2.5) is then solved using the FEM with a starting arbitrary value of D. Then, the solution c s compared to the reference concentration $\bar{c}$ (bottom. If the error is sufficiently small, the parameter D is the numerical optimum of the minimization problem (2.6), otherwise the value of D is updated and problem (2.5) is solved again to compute the new concentration c.

Here, a Tissue Chamber chip has been demonstrated for estimating the diffusion ability of nanoparticles under controlled biophysical conditions. First, the diffusion of FITC-Dextran molecules with three different molecular weights (4, 40 and 250 kDa) was assessed in a collagen gel using two different and independent techniques. The first approach is based on extracting the diffusion coefficient from the Mean Square Displacement (MSD). This is a very general technique that can be applied to molecules and nanoparticles. The second approach is based on the use of Fluorescence recovery After Photo-bleaching (FRAP), but this technique cannot be applied to nanoparticles. **Figure 2.2D** shows that the diffusion coefficients estimated with both techniques are in good agreement and no statistically significant difference is documented for all three tested Dextran molecules ($p = 0.118$ for 4 kDa dextran; $p = 0.426$ for 40 kDa dextran; and $p = 0.926$ for 250 kDa dextran). The FRAP technique is easier and more reliable then the MSD approach, as suggested by the smaller variations among the different measurements. The MSD technique is more cumbersome and reproducibility is more affected by the intrinsic higher difficulty associated with performing the experiments. Specifically, the channel diameter may vary slightly between experiments due to the fabrication process, the connection with external tubing or pipettes to the channel is not always optimal, and so on. Yet, FRAP and MSD return values for the diffusion coefficient that are in close agreement. This demonstrates the accuracy and reliability of the whole measurement protocol and the Tissue Chamber chip.

As FRAP cannot be applied to nanoparticles, the following measurements on SPNs and HA-Lip particles were performed using the MSD approach. **Figure 2.4** shows that the decoration of the nanoparticle surface with short PEG chains (2 kDa) increases their diffusivity in the collagen gel. This trend is indeed in agreement with the experimental

results presented by Zhang et al. (2017) [70]. In their work, the diffusion of two nanoparticles (65±3 nm bare cisplatin-loaded poly (aspartic acid) (PAA) particles and 74±2 nm PEGylated cisplatin-loaded PAA particles) was assessed within freshly excised healthy rat brain tissue slices. Under these conditions, Zhang and colleagues derived diffusion coefficients of the order of 10^{-3} $\mu m^2/s$ and 10^{-1} $\mu m^2/s$ for naked and PEGylated particles, respectively. Other authors have estimated the diffusion of PEGylate particles into mucus [80];[81]. Even in these works, the addition of PEG chains over a PLGA particle core improved diffusion. This was mainly ascribed to steric interactions arising at the interface between PEG chains and the surrounding mucus structure. More recently, Labouta et al. (2018) [82] showed that PEG density was the contributing factor in determining the penetration depth of liposome into collagen gels. Similarly, in this work the coating of spherical, solid polymeric nanoparticles with PEG (2 kDa) increases the mobility within the collagen gel, as compared to bare nanoparticles.

Following the same procedure of Zhang and colleagues, the diffusion of bare and PEGylated nanoparticles was also assessed in freshly excised brain tissue slides. The same behavior observed for the *in vitro* experiments were also documented *ex vivo*. Specifically, the nanoparticle diffusion increases with the surface density of the PEG chains. Indeed, the absolute values of the *ex vivo* diffusion coefficient are significantly smaller than those documented *in vitro*. This difference should be mostly attributed to three differences between the excised brain tissue and the Tissue Chamber chip, namely the presence of cells, the extracellular matrix composition, and the limited extracellular space that characterizes brain tissues [83]. It should be emphasized that it is difficult to perform a direct and objective comparison with previous results available in the literature because of differences in particle size and surface properties. Thorne and Nicholson [84]

measured, in living animals, the diffusivity of 35 nm quantum dots to be in the order of 10^{-1} $\mu m^2/s$. Zhang and colleagues [70] measured the diffusivity of 60 nm PAA particles to be in the order of 10^{-3} to 10^{-1} $\mu m^2/s$. In the current manuscript, the authors estimated the diffusivity of 200 nm particles to be in the order of 10^{-5} to 10^{-4} $\mu m^2/s$. These significant differences in diffusivity could be also ascribed to the significant difference in particle size.

In the case of hyaluronic acid-functionalized liposomes, the opposite trend was observed. Specifically, HA decoration over the liposome surface was responsible for a significant reduction in mobility. This decrease was directly related to HA molecular weight and possibly due to the entanglement of the long HA chains with the surrounding extracellular matrix. This macromolecular phenomenon may be driven by electrostatic forces [85] or by specific HA-collagen interactions [77];[86]. Importantly, even in the case of the HA-Lip, the *in vitro* trends are in full agreement with the *ex vivo* observations.

Taken all together, the data presented in this manuscript show that the proposed Tissue Chamber chip provides a versatile platform that can realize fundamental studies on particle diffusion in a tissue-like environment. Importantly, multiple biophysical parameters can be accurately controlled. For example, the tissue composition can be tailored to include collagen type I, type IV as well as hyaluronic acid, matrigel, other bio-macromolecules, and combinations thereof. Furthermore, the ECM can be modified to express specific adhesion molecules (e.g. integrins) or the density can be modified to affect the porosity of the tissue. Finally, cells could be included which could dynamically remodel the ECM, interact with the particles (uptake and trafficking) or act as physical barriers to particle transport. This platform can therefore be employed to conduct

systematic, comparative studies to evaluate nanoparticle transport processes in different recapitulated tissues. With such a tool it would be possible to optimize the geometrical and surface properties of nanoparticles to achieve high and uniform tissue penetration.

Chapter 3

3. A patient oriented colorectal cancer drug screening tool

3.1 Background

Cancer remains the leading cause of death in developed countries despite important progress has been made in understanding cancer biology and developing molecular target therapies. Usually, doctors rely on the histopathological staging of tumors and on molecular tests to evaluate the therapeutic strategy for each patient. Many efforts have been made to identify biomarkers that can predict a clinical response to specific treatments but only a few have demonstrated sufficient accuracy for use in clinical practice. A promising approach is to test the therapeutic efficacy of different drugs on cancer cells obtained from patients' tumor. Viable cancer cells can be isolated from freshly obtained tumor tissue and subsequently treated with drugs under controlled experimental conditions [87].

For example, colorectal cancer is one of the most frequently diagnosed cancers with more than 1.2 million new annual cases worldwide. Despite increasingly heavy therapies, overall 5-year survival is only about 60% in the western world. Cancer current treatments remain a challenge due to the heterogeneity of tumors originating from the same type of cells. This great heterogeneity makes it difficult for oncologists to structure an effective therapeutic strategy for the patient; 3D cultures represent a promising method for having a model of *in vitro* patient tumors therefore short term spheroid cell culture of colorectal

adenocarcinoma represents a promising *in vitro* model to use personalized medicine [87]. The need for the design of alternative therapies is therefore fundamental and this work aimed to define and validate an in vitro 3D culture system for the sensitivity test of primary colorectal cancer cells. The objectives of this part of work were to isolate primary colorectal cancer cells from patients' surgical resections and, from those, generate in vitro tumor spheroids resembling the heterogeneous population of the original tumor. In particular, the tumor spheroids were embedded in a matrix made of collagen type I as for the Tissue Chamber chip. This matrix was used to support the growth and sustenance of the spheroids and to ensure a favorable three-dimensional environment for growth and adaptation of the cells. In the effort to test the drug repurposing for radical therapies, the tumor spheroids obtained from different patients were subjected to the screening of aspirin and metformin. Aspirin is a drug that is usually used for cardiovascular disease and as anti-inflammatory drug [88] while metformin is a drug that is generally used for type 2 diabetes mellitus [89]. A 3D migration assay was performed in response to different dosages of MET, ASA and their combination. In particular, tumor spheroids were treated every other day for seven days with 5 and 10 mM. Furthermore, some markers were used in order to understand the effect of this drug at the molecular level.

3.2 Experimental procedure

Patient samples

The tissues were selected from 3 patients with colorectal cancer who underwent surgical resection of their primary tumors at the Genoa Galliera hospital. Furthermore, metastatic lymph nodes were taken from 3 other study-accessible patients. The fresh tumor tissues were collected by the anatomopathologist before the routine trials of the sample for diagnosis and staging. The supplied piece of tumor, was washed 3 times with water and 3 times with cold PBS (with Ca^{2+} and Mg^{2+}, sigma life science COD. D88662-500 ML) before being readily transported, on ice box, and in basic DMEM/F12 supplemented with a cocktail of antibiotics and antimycotics) to the laboratory of nanotechnology for the precision medicine at the IIT in Genoa. After the first macroscopic analysis and subsequent diagnosis, the tissue pieces found to be adenoma and non-adenocarcinoma were excluded from the study after receiving the pathology report. It is crucial for a successfully cell isolation to start the cells isolation as soon as the specimen is transported to the laboratory.

Spheroid preparation and culture

The spheroids have been prepared through an optimized protocol in our laboratory. The piece of tumor tissue was photographed and weighed operating in sterile conditions. Working in a biological hood, the piece is cut into small pieces of 1-2 mm size with razor blade and forceps. We took care to work on a small petri dish (35-60 mm) with cold medium (3-5 ml of basic DMEM/F12) covering the piece and laying down a polystyrene lid filled with ice and covered with aluminum foil. After removing the visibly fat parts and the necrotic ones, the mechanically fragmented material was pipetted up and down about ten times with a 5ml disposable pipet and placed into a 50 ml conical tube. Once placed in a falcon with a little volume of medium, the suspension was allowed to settle; the supernatant with small pieces of fat was removed. Now the tissue is started to the three enzymatic digestions using a complete cold medium: BASIC DMEM/F12 added with antibiotics and antimicotics, collagenase IV (GIBCO, 17104-019, 7.14 mg in 10 ml medium) and dnase I (Roche, cod.11284932001, 0.3-0.5 mg/ml). The tissue suspension was then kept for 45-60 minutes at 37 ° C taking care to pipet or vortex few times every 15 minutes to allow that mechanical dissociation acts with a synergistic effect to enzymatic digestion. After this time, the suspension was drawn with a 10 ml tip and then filtered through a 70 μm cell strainer (corning cell strainer 70 μm nylon REF 431751) previously wet with 1-2 ml of medium. From this first digestion it was thrown what goes through the filter, taking care to sift the pellet against the base of the filter with a piston of a 5ml syringe. At this point the filtrate was discarded and the indigested pieces present on the strainer were transferred to a new 50 ml conical tube. The pellet remained on the filter was taken with a 1000 μl tip and placed in another falcon filled with 10 ml medium

added with collagenase and dnase in the same way as the previous digestion step. At this point, after having pipetting the suspension, the falcon was placed again at 37 ° C for 45-60 minutes, always pipetting or vortexing every 15 minutes. Once this time has elapsed, the suspension was pipetted with a 10 ml tip and it was filtered again with a 70 μm filter previously wet with 1-2ml of medium. Also in this case the filtrate was thrown away and the pellet (the undigested pieces), before being placed again in a 50 ml falcon, it was sieved against the filter base using a 5 ml syringe plunger. At this point cell debris, extracellular matrix residues, blood cells and a few cancer cells get discarded through the filter. Also in this case the supernatant was thrown away and this pellet transferred into a 50 ml falcon with10 ml of an enzymatic solution of medium added with collagenase and dnase. The falcon underwent again 45-60 minutes at 37 ° C and at this point, the suspension was newly filtered with a 70 ul filter previously wetted with 1-2 ml of medium. Only now, the filtrate was maintained. The only difference is that now, the supernatant from this first filtration was filtered again with a 40 μl filter (corning cell strainer 40 um nylon REF 431750) previously wet with 1-2 ml of medium having care to wash the filter with 2 to 5 ml of medium. At this point tumor pieces were almost completely dissolved and cancer cells can be collected in the flow through. At this point, this filtrate from two consecutive filtrations was centrifuged for 10 min at 180 x g and the pellet suspended in 1 ml of complete medium and then an aliquot of cells was counted (10 μl) to be seeded in a 96 well plate low attachment for spheroid formation. 2000 cells/ well in a gravity trap TM ULA plate (insphero, ISP-09-001) (volume/ well is 70 μl), or 5000 cells/ well in a cell carrier TM- 96 spheroid ULA/CS (Perkin elmer, 6055330) (volume/well is 140 μl). To allow the best aggregation of the cells, the plates were centrifuged for 2 min at 250xg. Then, after replacing half of the old medium with fresh

complete medium every other day, the spheroid formation occurred between three and six days after seeding. Once generated, spheroids could be encapsulated in a collagen matrix. The protocol was optimized by placing 5000 cells in each well with 140 μl of complete medium and cultured at 37°C in a 5% CO_2 humidified incubator (Humidified incubator thermos scientific forma steri-cult CO_2 incubator). Note that, if from the second enzymatic digestion it can be seen no other tissue to be digested, third digestion could be avoid and the cell derived from the second one directly seeded. But, in that case, the suspension will be filtrate both with the 70 μm strainer and with the 40 μm one: it is the second filtrate that will be centrifuge, counted and seeded.

Spheroid formation

After 4-6 days of culture, the spheroids were mixed with a type I collagen solution (collagen solution from bovine skin, sigma life science) and gel mix solution in the ratio of 133 μl collagen, 34 μl gel mix solution e 33 μl culture medium with spheroid and seeded in 8 well plate with glass bottom useful for immunostaining and visualization under confocal microscopy (LAB TEK II Chambered coverglass w/cover#1.5 Borosilicate sterile 8 well 155409pk). The plates were incubated for one hour at 37 ° C to allow collagen polymerization. The spheroids were cultured for 4-6 days a 37°C in a 5% CO_2 humidified incubator and optical microscope images were recorded by a Leica DMI 6000 B with a 10X objective at day zero, day 4 and day 7 to follow the modification due to the treatment with drugs. The images were captured and the area of the spheroid

(i.e. the core and the spreading regions) were computed by imagej (https://imagej.nih.gov/).

Immunostaining

The immunostaining of the spheroids was done at day zero without any treatment, directly after an hour of incubation after seeding, just to wait the collagen gelation, and an hour after with complete medium only to highlight the stem cell and cancer cell biomarkers. ESA, CD133, CDX2, CK20 and β catenin were chosen to highlight cells characteristic proteins. 4 hours after treatment the proliferation and the inflammation through staining with Ki67 and COX2 were highlight. The same staining with Ki67 and COX2 was performed on the seventh day on another plate after zero day treatment, on day 4 and on day 7 with Metformin (MET) (SIGMA ALDRICH PHR 1084 500mg metformin hydrochloride) 10 mM, Aspirin (ASA) (Aspirin Sigma aldrich life science A 2093-100 G) 10 mM, and Aspirin-Metformin (ASAMET10) mM, plus, of course, the control with only medium without any drugs.

The immunostaining procedure starts with the gentle removing of the culture medium, washing three times with 200 µl PBS and then blocking with 200 µl of 4% PFA (paraformaldehyde Santa Cruz Biotechnology solutions 4% in PBS SC-781692) for 30 minutes at room temperature. Note that, only in the case in which it is involved the staining with CK20, the blocking must to be done with methanol (metOH), for 15 minutes at -20°C. After the blocking, PFA (or metOH) need to be removed and the gels washed with PBS, three times. After that, the membrane will be permeabilize with 200 µl of a triton solution (SIGMA T8787 100 ml) in PBS 0.1% (volume) for 30 minutes at room

temperature. After removed the permeabilizing agent, 200 µl di BSA (Bovine Serum Albumin Sigma Aldrich A7030-100 G) 5% were used to block aspecific sites for 1 h. After the BSA removal, 100 µl of a specific primary antibodies were added in a 3% BSA solution and incubated overnight under shaking at 4°C. In particular: Hoechst (cod. B2261 Sigma Aldrich) (1:500), Anti active b catenin (anti ABC) clone (8E7 05-665 EMD-Millipore corp., USA) (1:300) , CD323/EpCAM Ms anti-HU mAb clone VU-1D9, FITC conjugate (molecular probes life technologies REF A15755) (1:100) , Keratin 20 (D9Z1Z) XP (R) rabbit mAb (13063S cell signaling technology) (1:400) , CD133 (D2V8Q) (XP) (R) Rabbit mAb (64326S cell signaling technology) (1:400) , CDX2 (D11D10) Rabbit mAb (12306S cell signaling technology) (1:50) , Ki-67 (85D) Mouse mAb (944T cell signaling technology) (1:800) , COX2 (D5H5) XP (R) rabbit mAb (cell signaling technology) (1:800) in BSA 3% solution were put on the gel and incubated a 4 °C under shaking overnight. The day after, the removal of the primary antibodies and the washing with PBS three times during all the day, were followed by the incubation with 100 µl of a solution of secondary antibodies (all in ratio 1:500) in the incubation buffer incubated overnight at 4°C under shaking and protected from the light. The used secondary antibodies were Alexa fluor 488 Goat Anti Mouse IgG COD A11029 (Invitrogen), Alexa fluor 647 Goat anti rabbit cod A21245, Alexa fluor 568 A11036 Goat anti rabbit, Alexa fluor 568 goat anti mouse A11031, Alexa fluor 647 goat antimouse A21236 IgG. The day after, after the removal of the secondary antibodies solution and washing all the day three times with PBS, 1:500 Dapi (or Hoechst) in PBS was added to the gel and incubated at room temperature for 30 minutes protected from the light.

After washing three times with PBS without pose time, the samples were ready for the visualization. The staining was visualized by fluorescence confocal microscopy (Nikon

A1R confocal laser scanning microscope with a Plan Apo DIC N2) and the images were obtained with an objective10x.

3.3 Experimental results and discussion

For the work done, an integral part of a larger work in collaboration with the Galliera hospital in Genoa, the neoplasias (primary tumors) from three patients were analyzed, and from three other patient's metastatic lymph nodes were obtained, for a total of three primary neoplasias and three metastatic lymph nodes.

The spheroid heterogeneity was assessed using CD133 which is a transmembrane glycoprotein and EpCAM (ESA): both cancer stem cell markers. Moreover, the colon cancer biomarkers Ck20 and CDx2 are investigated. CK20 (cytokeratin 20) is a specific biomarker for colon cancer: antibodies to CK20 can be used to identify a range of adenocarcinoma arising from epithelia that normally contain the CK20 protein. Cytokeratins are located in the intracytoplasmic cytoskeleton of epithelial tissues and, for or example, the protein is commonly found in colorectal cancer. CDX2 is instead a nuclear marker especially for colorectal cancer. The Epithelial cell adhesion molecule (EpCAM) ESA is a transmembrane glycoprotein, used as cancer stem cell marker. Also, another marker, β-catenin was highlighted: mutations and overexpression of β-catenin are associated with many cancers, including colorectal carcinoma. Furthermore, a staining procedure was carried out for the proliferation marker Ki67 and the inflammation marker COX2; the Ki-67 antigen is a nuclear protein closely associated with cell proliferation and COX2 membrane protein overexpressed in several tumors, is related to inflammation state. The cellular composition of the spheroids was evaluated with the immunostaining

at day zero without treatment: as can be seen the tumor and stem cell markers identify the region of stemness in the center and the cancer cells outside, as can be seen from the **Figure 3.1**.

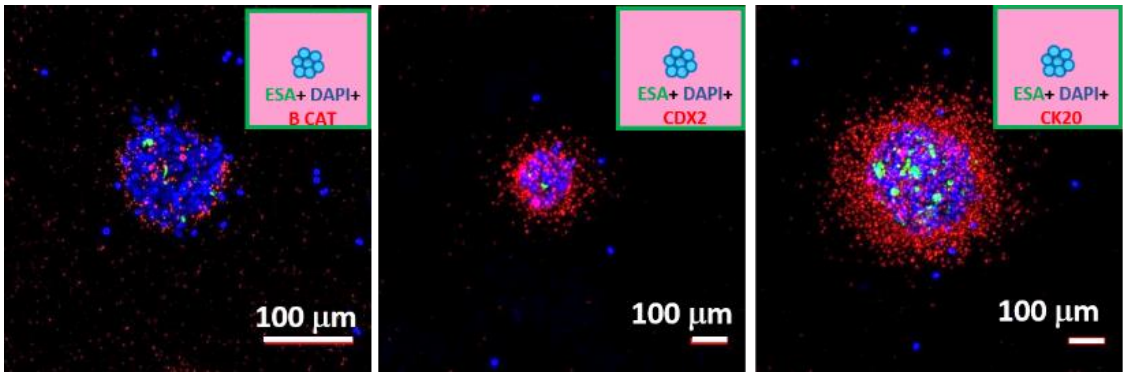

Figure 3.1 *Fluorescent confocal microscopy images of spheroids labeled with the biomarker ESA (green), CDX2 (red), β CATENIN (red), CK20 (red) and DAPI (blue, nuclei) at the day 0, without treatment.*

To investigate the molecular action of metformin and aspirin on metabolism and inflammation respectively, COX2 and Ki-67 staining were done on day zero after 4 hours of treatment for short term therapy and on day 7 after treatment each other days as can be seen from the **Figures 3.2-3.3** which show that metformin and aspirin reduced the proliferation and the inflammation.

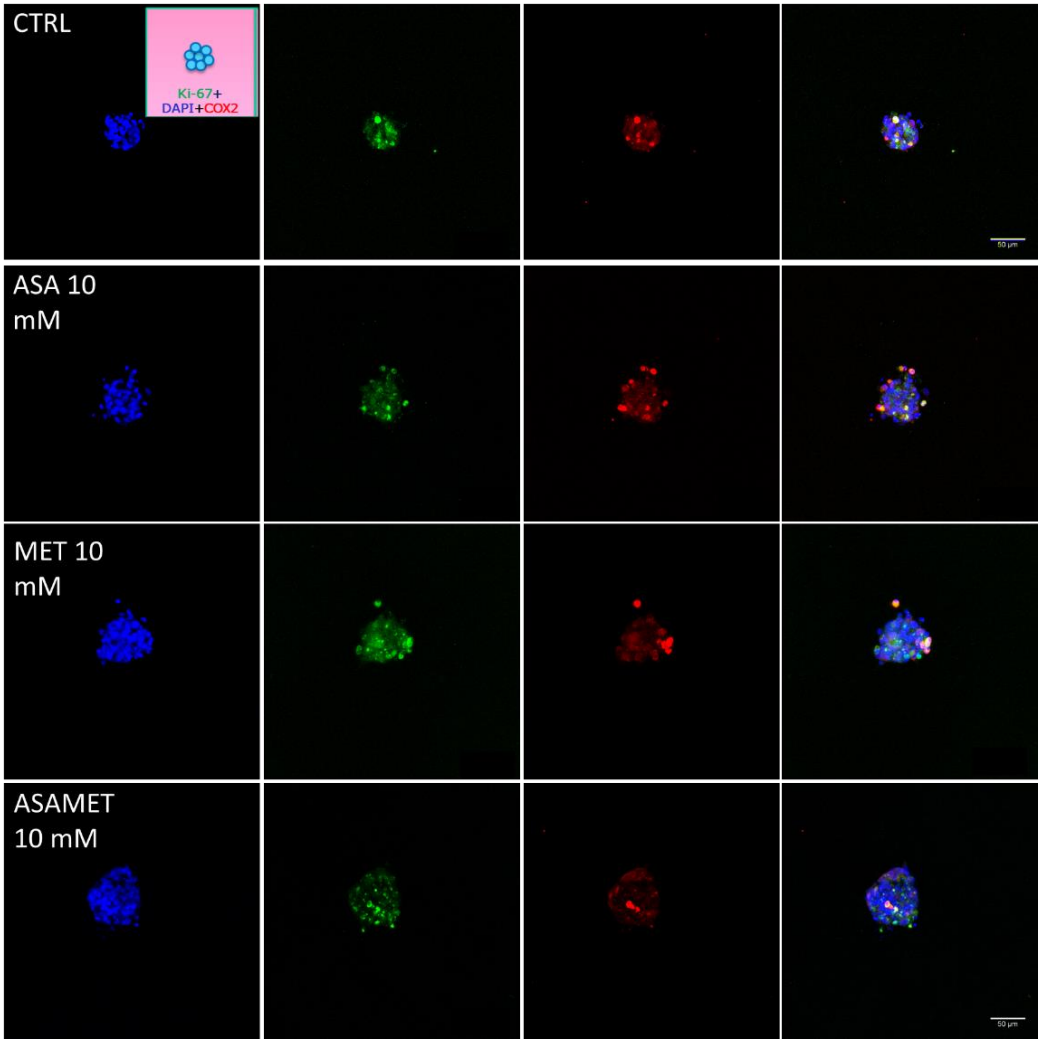

Figure 3.2 *Fluorescent confocal microscopy images of spheroid labeled with the biomarkers Ki-67 (green), COX2 (red) and DAPI (blue, nuclei) at the day 0, after 4 hour of treatment. Scale bar are 50 μm.*

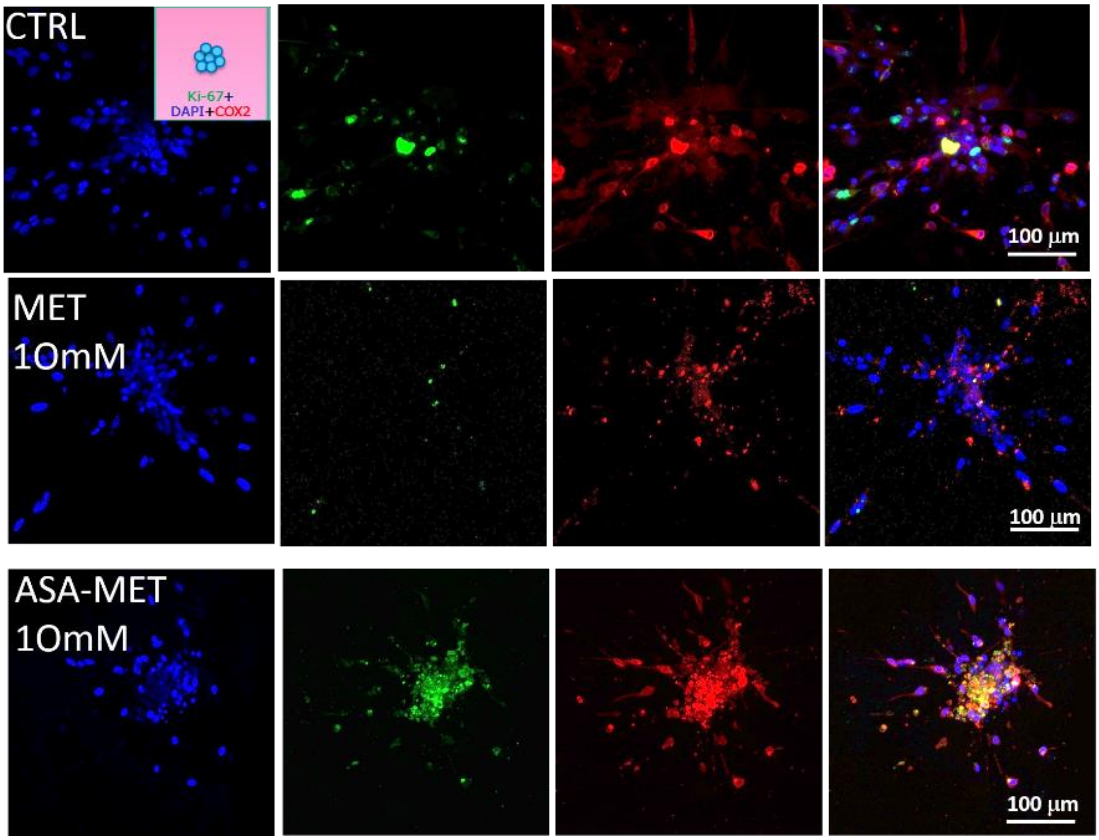

Figure 3.3 *Fluorescent confocal microscopy images of spheroid labeled with the biomarkers Ki-67 (green), COX2 (red) and DAPI (blue, nuclei) at the day 7, after 7 days of treatment each other day.*

In **Figure 3.4** it is possible to see the piece of the tissue and the schematic of how the process takes place from obtaining the piece to processing till cells isolation, in order to seed them in the 96 low attachment well plates.

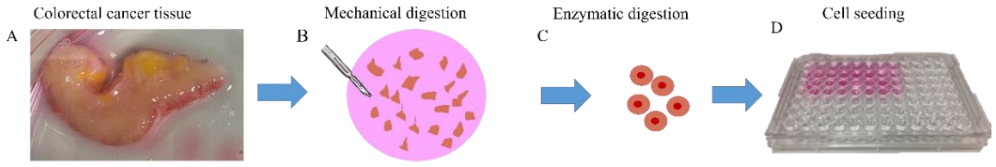

Figure* 3.4 *Spheroid obtaining from biopsies of colorectal cancer. *A. biopsy obtained from the Galliera hospital. B. mechanical fragmentation of the tissue. C. Enzymatic digestion. D. Cell seeded in 96 low-attachment well plate.*

After 4-6 days the spheroids were placed in the collagen matrix (**Figure 3.5-3.6-3.7)** and were treated on alternate days with metformin, aspirin and combination of the two at concentrations of 5 mM, and 10 mM.

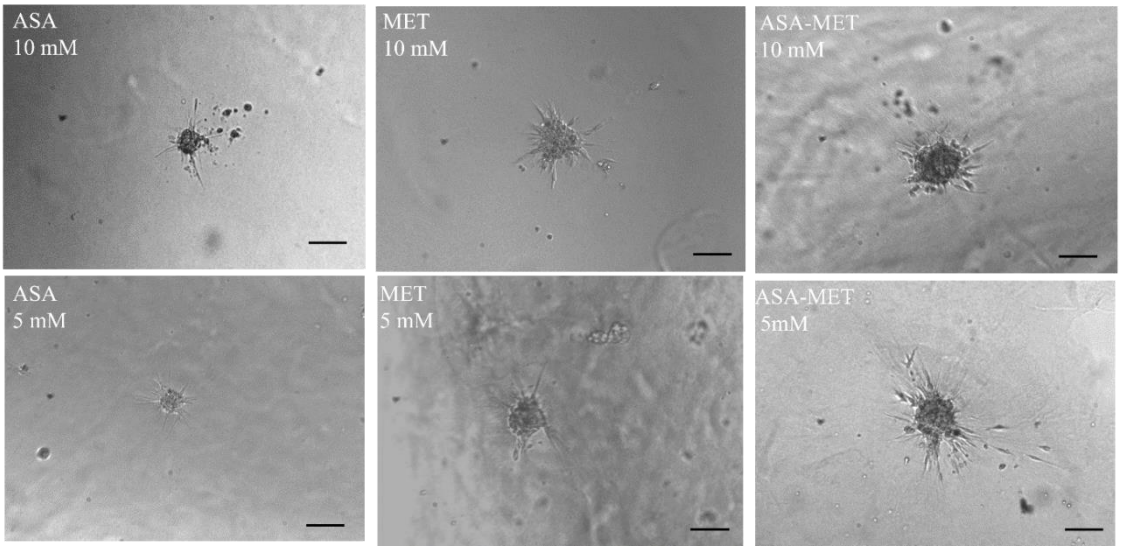

Figure 3.5 *Spheroids from primary colorectal cancer responded to treatment at day 1. Scale bar are 100 μm.*

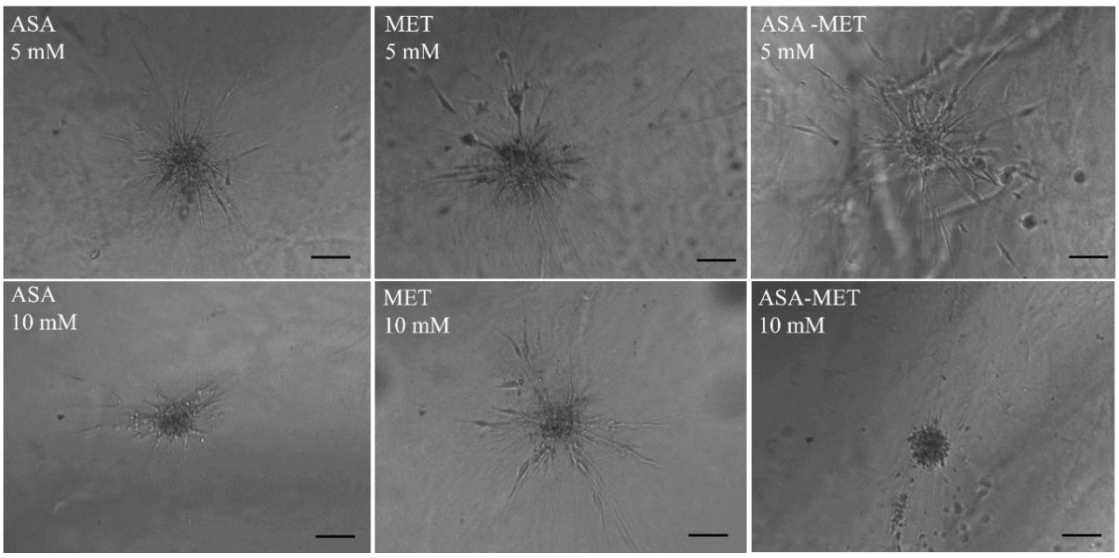

Figure 3.6 *Spheroids from primary colorectal cancer responded to treatment at day 4. Scale bar are 100 μm.*

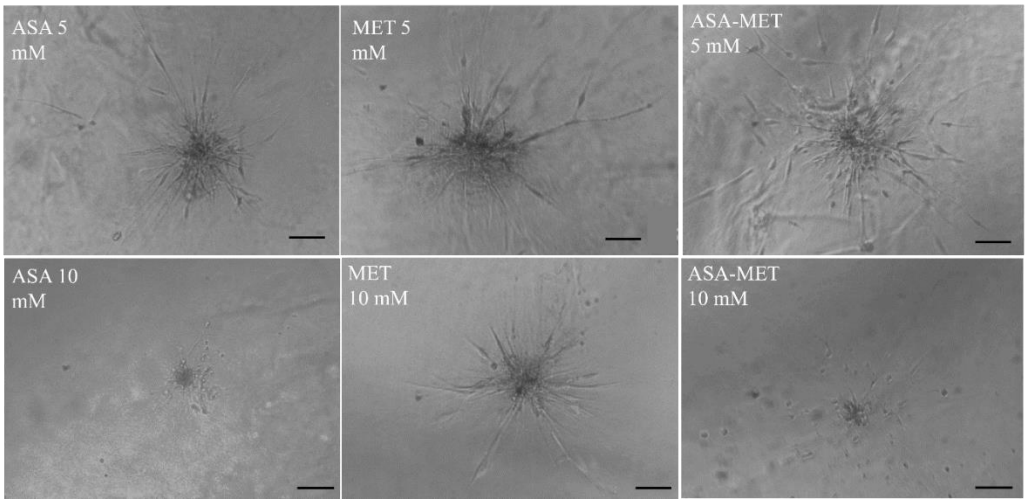

Figure 3.7 *Spheroids from primary colorectal cancer responded to treatment at day 7. Scale bar are 100 μm.*

We proceeded to calculate the core and the external migration region on days 1, 4 and 7 and the difference between the outer radius and the inner radius were plotted as can be seen from the graphs in **Figure 3.8-3.9**. From these graphs, both those for the primary tumor (**Figure 3.8**) and those for the metastatic lymph node (**Figure 3.9**) it is clear that the greatest action on migration was given by aspirin and by the combination aspirin and metformin, and in both cases the best effect has been obtained at 10 mM.

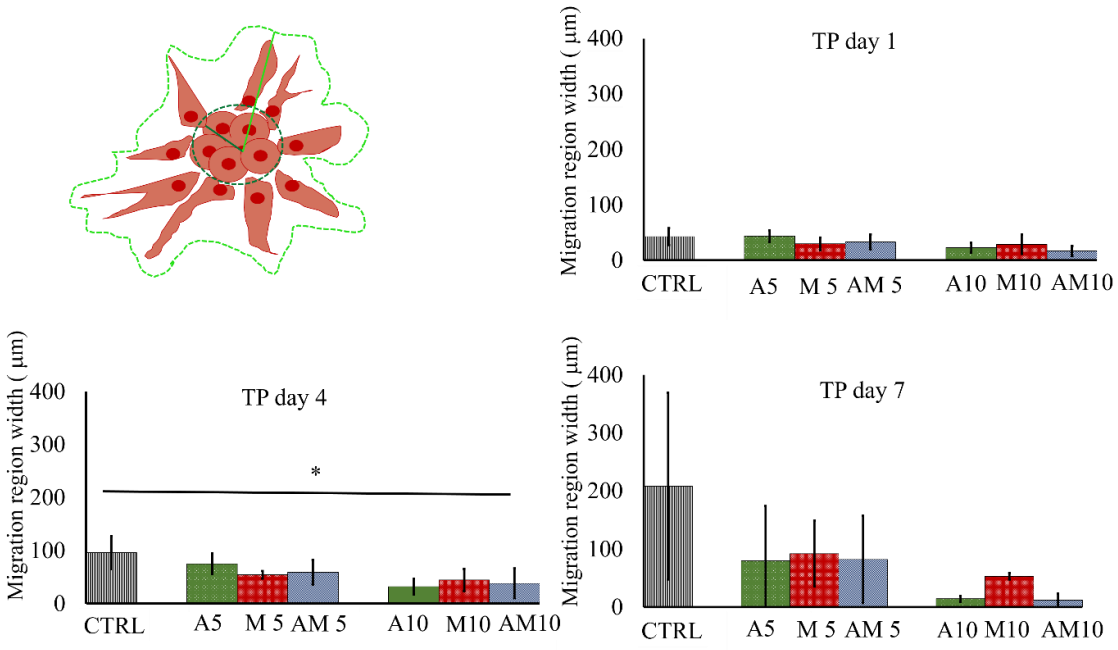

Figure 3.8 Primary tumor spheroid migration assay*. A. Cartoon of the spheroid in which the core and the external migration region are represented. The graphs show the trend on day 1 (figure B), on day 4 (figure C) and on day 7 (figure D) treated with different drug concentrations (Aspirin 5 mM and 10 mM, Metformin 5 mM and 10 mM and their combinations) compared with control at various days. Anova test * = p <0.05, n = 3*

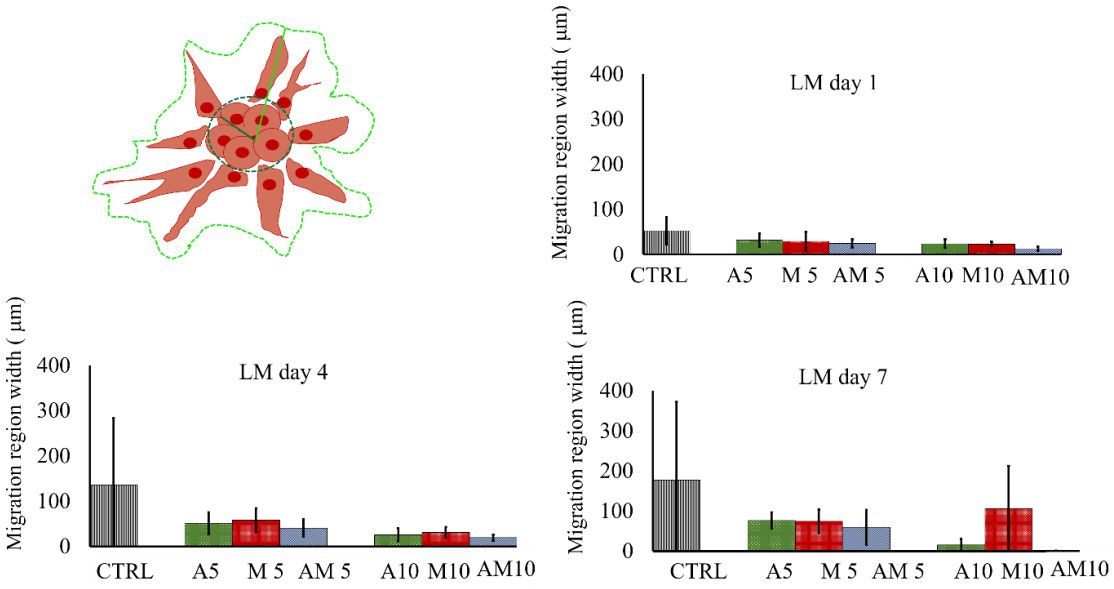

Figure 3.9 Migration assay of spheroids from metastatic lymph nodes*. A. Cartoon of the spheroid in which the core and the external migration region are represented. The graphs show the trend on day 1 (figure B), on day 4 (figure C) and on day 7 (figure D) treated with different drug concentrations (Aspirin 5 mM and 10 mM, Metformin 5 mM and 10 mM and their combinations) compared with control at various days. Anova test * = p <0.05, n = 3 patients.*

The development of a functional assay to predict the sensitivity of individuals' tumors is important to increase the clinical response success. 3D cancer cultures are considered to reflect the condition of in vivo tumors more closely than in traditional 2D cultures and therefore represent a promising system for chemosensitivity tests [87].

In this study, colorectal cancer cells were isolated from tumor fragments and cultured in 3D as spheroids. The spheroid characterization showed that the heterogeneity and characteristics of the colorectal cancer were maintained during the short-term culture (7 days) in an in vitro culture. Staining confirmed that the spheroids consist of neoplastic cells of epithelial derivation. What has been noticed is that the spheroids growth does not depend on the size of the isolated tumor fragments. Therefore, these results indicate that all the dimensions of the investigated spheroids can be used to test growth and inhibition growth as a measure of drug sensitivity. Thus, it was shown that the primary colorectal 3D cultures showed a number of features found in the original tumors. The histological staining of the obtained cultures confirmed that the spheroids maintain the characteristics of the colorectal adenocarcinoma.

Chapter 4

Conclusions and future perspectives

One of the reasons why chemotherapy, and more specifically any type of drug, fails in its effectiveness is the difficulty to reach the site of action and reaching it at the necessary concentration. The achievement of the site of action at the right concentration was addressed using nanoparticles. These vectors are considered as drugs transporters to the tumor site thanks to the EPR effect that exploits the fenestrations of the tumor blood vessels to accumulate at the site of the tumor itself. They also can exploit a target surface functionalization to bind only to cancer cells and avoid side effects gave from the effect of these drugs on healthy tissues. It is very important, in the perspective of a personalized therapy and in view of a precision medicine, to understand how long certain drug carriers manage to reach the action site. It is therefore important to understand how much surface these substances and nanoparticles or free drugs can cover in the unit of time. For this issue, different nanoparticles with different surface functionalization have been studied for their diffusion. The attention was focused on particles of the same size, 200 nm, and their movement over time within two different substrates were studied. The first substrate was represented by a collagen matrix that is the main component of the extracellular matrix. A second substrate was instead represented by mice brain slices to have a real tissue and a greater complexity than the simple collagen. Within these tissues, particles of different composition and different surface functionalization were injected. It has been seen that polymeric spherical particles had a greater diffusion when these were

functionalized with a higher percentage of polyethylene glycol that acts as a lubricating agent. On the other hand, 200 nm liposomes have been functionalized with two different molecular weights hyaluronic acid: 5kDa and 700kDa. What has been noticed was that hyaluronic acid has the opposite effect compared to polyethylene glycol. The particles not covered with hyaluronic acid showed the greatest diffusion, while among those covered with hyaluronic acid, those ones with 700kDa had the most hampered diffusion probably due to the effect of entanglement with collagen fibers. These results emerged both from the collagen matrix and from the murine brain matrix, although the brain slices offered greater resistance to diffusion due to their characteristics histology and architecture.

The next step, to get even closer to a model similar to the reality that allows ever more translational research, was to study the diffusion of these same carriers within a human tissue, in this case cancerous one, starting exactly from tumor biopsies. In this regard, a protocol has been optimized to obtain spheroids that resemble human cancer tissue starting precisely from these biopsies. The aim of this third part of the work was to recreate the heterogeneity of the colorectal cancer human tissue and proceed with immunostaining to understand how the spheroid was made. Moreover, the effect of two drugs already in the clinical study at the Galliera Hospital were analyzed in order to have a tool to use as drug screening. The ASAMET clinical study, uses Aspirin, Metformin and the combination of these two drugs that usually are used for different pathologies. These therapeutics were used as adjuvant therapy of primary colorectal cancer after the surgical operation to avoid relapse. But, if the ASAMET clinical trial will gave us good results, this combination of drug could be use also to treat metastasis and not only to avoiding of relapse. Our spheroids gave us these results, namely ASAMET was the best

solution to affect the migration reducing tumoral cells spreading. So, understanding that with this kind of tool, it was possible to resemble what usually happens in the clinical trials, this tool could be effectively used to predicts patients' outcomes and to address other clinical studies more in the details. In the future, nanoparticles and free drugs will be tested on this device to understand other characteristic that a carrier needs to have to penetrate within a tumoral mass and influence their growth. The final aim will be to translate as soon as possible this new carrier to the clinics and to address more and more the precision nanomedicine vision.

References

1. Holback, H. and Y. Yeo, *Intratumoral drug delivery with nanoparticulate carriers.* Pharmaceutical research, 2011. **28**(8): p. 1819-1830.
2. Jain, R.K. and T. Stylianopoulos, *Delivering nanomedicine to solid tumors.* Nature reviews Clinical oncology, 2010. **7**(11): p. 653.
3. Erikson, A., et al., *Physical and chemical modifications of collagen gels: impact on diffusion.* Biopolymers: Original Research on Biomolecules, 2008. **89**(2): p. 135-143.
4. Seo, B.R., P. DelNero, and C. Fischbach, *In vitro models of tumor vessels and matrix: engineering approaches to investigate transport limitations and drug delivery in cancer.* Advanced drug delivery reviews, 2014. **69**: p. 205-216.
5. Karim, R., et al., *Nanocarriers for the treatment of glioblastoma multiforme: current state-of-the-art.* Journal of controlled release, 2016. **227**: p. 23-37.
6. Stylianopoulos, T., et al., *Diffusion of particles in the extracellular matrix: the effect of repulsive electrostatic interactions.* Biophysical journal, 2010. **99**(5): p. 1342-1349.
7. Drost, J. and H. Clevers, *Organoids in cancer research.* Nature Reviews Cancer, 2018. **18**(7): p. 407.
8. Peer, D., et al., *Nanocarriers as an emerging platform for cancer therapy.* Nature nanotechnology, 2007. **2**(12): p. 751.
9. Ferrari, M., *Cancer nanotechnology: opportunities and challenges.* Nature reviews cancer, 2005. **5**(3): p. 161.

10. Khodabandehloo, H., H. Zahednasab, and A.A. Hafez, *Nanocarriers usage for drug delivery in cancer therapy.* Iranian journal of cancer prevention, 2016. **9**(2).
11. Bernal, G.M., et al., *Convection-enhanced delivery and in vivo imaging of polymeric nanoparticles for the treatment of malignant glioma.* Nanomedicine: Nanotechnology, Biology and Medicine, 2014. **10**(1): p. 149-157.
12. Rosenblum, D., et al., *Progress and challenges towards targeted delivery of cancer therapeutics.* Nature communications, 2018. **9**(1): p. 1410.
13. Shi, J., et al., *Cancer nanomedicine: progress, challenges and opportunities.* Nature Reviews Cancer, 2017. **17**(1): p. 20.
14. Nabil, G., et al., *Nano-engineered delivery systems for cancer imaging and therapy: Recent advances, future direction and patent evaluation.* Drug discovery today, 2019. **24**(2): p. 462-491.
15. Arranja, A.G., et al., *Tumor-targeted nanomedicines for cancer theranostics.* Pharmacological research, 2017. **115**: p. 87-95.
16. Moore, T.L., et al., *Polymer-Coated Radioluminescent Nanoparticles for Quantitative Imaging of Drug Delivery.* Advanced Functional Materials, 2014. **24**(37): p. 5815-5823.
17. Blanco, E., et al., *Colocalized delivery of rapamycin and paclitaxel to tumors enhances synergistic targeting of the PI3K/Akt/mTOR pathway.* Molecular Therapy, 2014. **22**(7): p. 1310-1319.
18. Pushpalatha, R., S. Selvamuthukumar, and D. Kilimozhi, *Nanocarrier mediated combination drug delivery for chemotherapy–A review.* Journal of Drug Delivery Science and Technology, 2017. **39**: p. 362-371.

19. Tietjen, G.T., et al., *Focus on fundamentals: achieving effective nanoparticle targeting.* Trends in molecular medicine, 2018. **24**(7): p. 598-606.

20. Lazarovits, J., et al., *Nanoparticle–blood interactions: the implications on solid tumour targeting.* Chemical Communications, 2015. **51**(14): p. 2756-2767.

21. Wilhelm, S., et al., *Analysis of nanoparticle delivery to tumours.* Nature reviews materials, 2016. **1**(5): p. 16014.

22. Hua, S., et al., *Current trends and challenges in the clinical translation of nanoparticulate nanomedicines: pathways for translational development and commercialization.* Frontiers in pharmacology, 2018. **9**.

23. Blanco, E., H. Shen, and M. Ferrari, *Principles of nanoparticle design for overcoming biological barriers to drug delivery.* Nature biotechnology, 2015. **33**(9): p. 941.

24. Cabral, H., et al., *Accumulation of sub-100 nm polymeric micelles in poorly permeable tumours depends on size.* Nature nanotechnology, 2011. **6**(12): p. 815.

25. Wong, C., et al., *Multistage nanoparticle delivery system for deep penetration into tumor tissue.* Proceedings of the National Academy of Sciences, 2011. **108**(6): p. 2426-2431.

26. Tasciotti, E., et al., *Mesoporous silicon particles as a multistage delivery system for imaging and therapeutic applications.* Nature nanotechnology, 2008. **3**(3): p. 151.

27. Hu, C.-M.J., et al., *Erythrocyte membrane-camouflaged polymeric nanoparticles as a biomimetic delivery platform.* Proceedings of the National Academy of Sciences, 2011. **108**(27): p. 10980-10985.

28. Pitchaimani, A., et al., *Biomimetic Natural Killer Membrane Camouflaged Polymeric Nanoparticle for Targeted Bioimaging.* Advanced Functional Materials, 2019. **29**(4): p. 1806817.

29. Anselmo, A.C., et al., *Monocyte-mediated delivery of polymeric backpacks to inflamed tissues: a generalized strategy to deliver drugs to treat inflammation.* Journal of controlled release, 2015. **199**: p. 29-36.

30. Brenner, J.S., et al., *Red blood cell-hitchhiking boosts delivery of nanocarriers to chosen organs by orders of magnitude.* Nature communications, 2018. **9**(1): p. 2684.

31. Choi, M.-R., et al., *Delivery of nanoparticles to brain metastases of breast cancer using a cellular Trojan horse.* Cancer nanotechnology, 2012. **3**(1): p. 47.

32. Moore, T.L., et al., *Cellular shuttles: monocytes/macrophages exhibit transendothelial transport of nanoparticles under physiological flow.* ACS applied materials & interfaces, 2017. **9**(22): p. 18501-18511.

33. Zhang, W., et al., *Nanoparticle-Laden Macrophages for Tumor-Tropic Drug Delivery.* Advanced Materials, 2018. **30**(50): p. 1805557.

34. Bhise, N.S., et al., *Organ-on-a-chip platforms for studying drug delivery systems.* Journal of Controlled Release, 2014. **190**: p. 82-93.

35. Mouw, J.K., G. Ou, and V.M. Weaver, *Extracellular matrix assembly: a multiscale deconstruction.* Nature reviews Molecular cell biology, 2014. **15**(12): p. 771.

36. Theocharis, A.D., et al., *Extracellular matrix structure.* Advanced drug delivery reviews, 2016. **97**: p. 4-27.

37. Gill, B.J. and J.L. West, *Modeling the tumor extracellular matrix: Tissue engineering tools repurposed towards new frontiers in cancer biology.* Journal of biomechanics, 2014. **47**(9): p. 1969-1978.

38. Hess, M.W., et al., *3D versus 2D cell culture: implications for electron microscopy*, in *Methods in cell biology*. 2010, Elsevier. p. 649-670.

39. Hardelauf, H., et al., *Microarrays for the scalable production of metabolically relevant tumour spheroids: a tool for modulating chemosensitivity traits.* Lab on a Chip, 2011. **11**(3): p. 419-428.

40. Mehta, G., et al., *Opportunities and challenges for use of tumor spheroids as models to test drug delivery and efficacy.* Journal of Controlled Release, 2012. **164**(2): p. 192-204.

41. Edmondson, R., et al., *Three-dimensional cell culture systems and their applications in drug discovery and cell-based biosensors.* Assay and drug development technologies, 2014. **12**(4): p. 207-218.

42. Lee, J., et al., *In vitro toxicity testing of nanoparticles in 3D cell culture.* Small, 2009. **5**(10): p. 1213-1221.

43. Sontheimer-Phelps, A., B.A. Hassell, and D.E. Ingber, *Modelling cancer in microfluidic human organs-on-chips.* Nature Reviews Cancer, 2019: p. 1.

44. Stylianopoulos, T., et al., *Diffusion anisotropy in collagen gels and tumors: the effect of fiber network orientation.* Biophysical journal, 2010. **99**(10): p. 3119-3128.

45. Ramanujan, S., et al., *Diffusion and convection in collagen gels: implications for transport in the tumor interstitium.* Biophysical journal, 2002. **83**(3): p. 1650-1660.

46. Meyvis, T.K., et al., *Fluorescence recovery after photobleaching: a versatile tool for mobility and interaction measurements in pharmaceutical research.* Pharmaceutical research, 1999. **16**(8): p. 1153-1162.

47. Elson, E.L. and D. Magde, *Fluorescence correlation spectroscopy. I. Conceptual basis and theory.* Biopolymers: Original Research on Biomolecules, 1974. **13**(1): p. 1-27.

48. Krichevsky, O. and G. Bonnet, *Fluorescence correlation spectroscopy: the technique and its applications.* Reports on Progress in Physics, 2002. **65**(2): p. 251.

49. Bacia, K., S.A. Kim, and P. Schwille, *Fluorescence cross-correlation spectroscopy in living cells.* Nature methods, 2006. **3**(2): p. 83.

50. Wlodkowic, D. and J.M. Cooper, *Tumors on chips: oncology meets microfluidics.* Current opinion in chemical biology, 2010. **14**(5): p. 556-567.

51. Elliott, N.T. and F. Yuan, *A microfluidic system for investigation of extravascular transport and cellular uptake of drugs in tumors.* Biotechnology and bioengineering, 2012. **109**(5): p. 1326-1335.

52. Hou, J., et al., *A novel chemotherapeutic sensitivity-testing system based on collagen gel droplet embedded 3D–culture methods for hepatocellular carcinoma.* Bmc Cancer, 2017. **17**(1): p. 729.

53. Katt, M.E., et al., *In vitro tumor models: advantages, disadvantages, variables, and selecting the right platform.* Frontiers in bioengineering and biotechnology, 2016. **4**: p. 12.

54. Shamir, E.R. and A.J. Ewald, *Three-dimensional organotypic culture: experimental models of mammalian biology and disease.* Nature reviews Molecular cell biology, 2014. **15**(10): p. 647.

55. van de Wetering, M., et al., *Prospective derivation of a living organoid biobank of colorectal cancer patients.* Cell, 2015. **161**(4): p. 933-945.

56. Vlachogiannis, G., et al., *Patient-derived organoids model treatment response of metastatic gastrointestinal cancers.* Science, 2018. **359**(6378): p. 920-926.

57. Mozar, F.S. and E.H. Chowdhury, *Impact of PEGylated nanoparticles on tumor targeted drug delivery.* Current pharmaceutical design, 2018. **24**(28): p. 3283-3296.

58. Sun, T., et al., *Engineered nanoparticles for drug delivery in cancer therapy.* Angewandte Chemie International Edition, 2014. **53**(46): p. 12320-12364.

59. Lee, A., et al., *Spherical polymeric nanoconstructs for combined chemotherapeutic and anti-inflammatory therapies.* Nanomedicine: Nanotechnology, Biology and Medicine, 2016. **12**(7): p. 2139-2147.

60. Mizrahy, S., et al., *Tumor targeting profiling of hyaluronan-coated lipid based-nanoparticles.* Nanoscale, 2014. **6**(7): p. 3742-3752.

61. Peer, D. and R. Margalit, *Physicochemical evaluation of a stability-driven approach to drug entrapment in regular and in surface-modified liposomes.* Archives of biochemistry and biophysics, 2000. **383**(2): p. 185-190.

62. Peer, D. and R. Margalit, *Loading mitomycin C inside long circulating hyaluronan targeted nano-liposomes increases its antitumor activity in three mice tumor models.* International Journal of Cancer, 2004. **108**(5): p. 780-789.

63. Peer, D., et al., *Systemic leukocyte-directed siRNA delivery revealing cyclin D1 as an anti-inflammatory target.* Science, 2008. **319**(5863): p. 627-630.

64. Kedmi, R., N. Ben-Arie, and D. Peer, *The systemic toxicity of positively charged lipid nanoparticles and the role of Toll-like receptor 4 in immune activation.* Biomaterials, 2010. **31**(26): p. 6867-6875.

65. Landesman-Milo, D., et al., *Hyaluronan grafted lipid-based nanoparticles as RNAi carriers for cancer cells.* Cancer letters, 2013. **334**(2): p. 221-227.

66. Valentine, M., et al., *Colloid surface chemistry critically affects multiple particle tracking measurements of biomaterials.* Biophysical journal, 2004. **86**(6): p. 4004-4014.

67. Michalet, X., *Mean square displacement analysis of single-particle trajectories with localization error: Brownian motion in an isotropic medium.* Physical Review E, 2010. **82**(4): p. 041914.

68. Tröltzsch, F., *Optimal control of partial differential equations: theory, methods, and applications*. Vol. 112. 2010: American Mathematical Soc.

69. Sancataldo, G., et al., *Three-dimensional multiple-particle tracking with nanometric precision over tunable axial ranges.* Optica, 2017. **4**(3): p. 367-373.

70. Zhang, C., et al., *Convection enhanced delivery of cisplatin-loaded brain penetrating nanoparticles cures malignant glioma in rats.* Journal of Controlled Release, 2017. **263**: p. 112-119.

71. Schindelin, J., et al., *Fiji: an open-source platform for biological-image analysis.* Nature methods, 2012. **9**(7): p. 676.

72. Armstrong, J.K., et al., *The hydrodynamic radii of macromolecules and their effect on red blood cell aggregation.* Biophysical journal, 2004. **87**(6): p. 4259-4270.

73. Stigliano, C., et al., *Radiolabeled polymeric nanoconstructs loaded with docetaxel and curcumin for cancer combinatorial therapy and nuclear imaging.* Advanced Functional Materials, 2015. **25**(22): p. 3371-3379.

74. Essa, S., J.M. Rabanel, and P. Hildgen, *Characterization of rhodamine loaded PEG-g-PLA nanoparticles (NPs): effect of poly (ethylene glycol) grafting density.* International journal of pharmaceutics, 2011. **411**(1-2): p. 178-187.

75. Wolfram, J., et al., *Shrinkage of pegylated and non-pegylated liposomes in serum.* Colloids and Surfaces B: Biointerfaces, 2014. **114**: p. 294-300.

76. Dancy, J.G., et al., *Non-specific binding and steric hindrance thresholds for penetration of particulate drug carriers within tumor tissue.* Journal of Controlled Release, 2016. **238**: p. 139-148.

77. Annabi, B., et al., *Hyaluronan cell surface binding is induced by type I collagen and regulated by caveolae in glioma cells.* Journal of Biological Chemistry, 2004. **279**(21): p. 21888-21896.

78. Mizrahy, S., et al., *Hyaluronan-coated nanoparticles: the influence of the molecular weight on CD44-hyaluronan interactions and on the immune response.* Journal of controlled release, 2011. **156**(2): p. 231-238.

79. Tinevez, J.-Y., et al., *TrackMate: An open and extensible platform for single-particle tracking.* Methods, 2017. **115**: p. 80-90.

80. Cu, Y. and W.M. Saltzman, *Controlled surface modification with poly (ethylene) glycol enhances diffusion of PLGA nanoparticles in human cervical mucus.* Molecular pharmaceutics, 2008. **6**(1): p. 173-181.

81. Xu, Q., et al., *Impact of surface polyethylene glycol (PEG) density on biodegradable nanoparticle transport in mucus ex vivo and distribution in vivo.* ACS nano, 2015. **9**(9): p. 9217-9227.

82. Labouta, H.I., et al., *Surface-grafted polyethylene glycol conformation impacts the transport of PEG-functionalized liposomes through a tumour extracellular matrix model.* RSC advances, 2018. **8**(14): p. 7697-7708.

83. Syková, E. and C. Nicholson, *Diffusion in brain extracellular space.* Physiological reviews, 2008. **88**(4): p. 1277-1340.

84. Thorne, R.G. and C. Nicholson, *In vivo diffusion analysis with quantum dots and dextrans predicts the width of brain extracellular space.* Proceedings of the National Academy of Sciences, 2006. **103**(14): p. 5567-5572.

85. Gelman, R.A. and J. Blackwell, *Collagen-mucopolysaccharide interactions at acid pH.* Biochimica et Biophysica Acta (BBA)-Protein Structure, 1974. **342**(2): p. 254-261.

86. McDevitt, C.A., J. Marcelino, and L. Tucker, *Interaction of intact type VI collagen with hyaluronan.* FEBS letters, 1991. **294**(3): p. 167-170.

87. Jeppesen, M., et al., *Short-term spheroid culture of primary colorectal cancer cells as an in vitro model for personalizing cancer medicine.* PloS one, 2017. **12**(9): p. e0183074.

88. Ridker, P.M., et al., *Inflammation, aspirin, and the risk of cardiovascular disease in apparently healthy men.* New England journal of medicine, 1997. **336**(14): p. 973-979.

89. Inzucchi, S.E., et al., *Efficacy and metabolic effects of metformin and troglitazone in type II diabetes mellitus.* New England Journal of Medicine, 1998. **338**(13): p. 867-873.